Gelasia Tomentosa Butanolic Extract Exhibits Antiproliferative Activity Against MCF-7 Breast Cancer Cells: Mechanistic Insights into Synergistic EGFR and TOP2A Targeting

Amjed Abbawe Salih[1], Amenh Mohammed Abdulrahman[2], Ali Mala Khedir Galalaey[3], Waleed Khalid Ahmed[4], Shatha H. Shaker[5], Youssef Shakuri Yasin[6,*], Ahmed Mohsin Abdulkhadim[7] and Azal Hamoody Jumaa[8]

[1]*College of Dentistry, Kirkuk University, Iraq*

[2]*Al-Iraqia University, College of Medicine, Department of Pharmacology, Baghdad, Iraq*

[3]*College of Agricultural Engineering Sciences, University of Salahaddin-Erbil, Kurdistan Region, Iraq*

[4]*Department of Chemistry and Biochemistry, College of Medicine, University of Fallujah, Iraq*

[5]*Department of Biology, College of Education for Pure Sciences, Tikrit University, Iraq*

[6]*Bilad Alrafidain University, Iraq*

[7]*Kamal Al-Samarrai Hospital, Ministry of Health, Iraq*

[8]*Iraqi National Cancer Research Center/University of Baghdad, Iraq*

Abstract: *Objective*: This preliminary study investigated the *in vitro* cytotoxicity and selectivity of the Gelasia tomentosa butanolic extract (Gt-BuOH) against MCF-7 breast cancer cells, using HFF fibroblasts as a non-malignant control, and explored associations between treatment and changes in p-EGFR, TOP2A, and TNF-α protein levels. Molecular docking was performed to generate hypotheses.

Materials and Methods: Gt-BuOH (13.6% w/w fatty extract) was prepared by liquid-liquid partitioning of 650 g of powdered aerial parts. Chemical composition was characterized by GC-MS with retention index matching; compounds with similarity index ≥70% were tentatively identified. Cytotoxicity was determined using the MTT assay for cell viability at 0.1–1000 µg/mL in the MCF-7 cancer cell line and healthy HFF cells after 24 h and 72 h of incubation. Quantification of p-EGFR, TOP2A, and TNF-α was performed by ELISA. Key phytoconstituents were docked against these targets, with binding affinities estimated using AutoDock Vina.

Results: Gt-BuOH inhibited MCF-7 cells in a concentration- and time-dependent manner (2.0 ± 0.2% to 75.0 ± 0.3% at 72 h; IC_{50} = 431.8 µg/mL) with low toxicity towards HFF (IC_{50} > 1000 µg/mL; selectivity index > 2.32). GC-MS identified methyl oleate (71.62% of total ion chromatogram area), propanoic anhydride, and methyl butyrate as the principal constituents; the profile is dominated by fatty-acid derivatives rather than phenolics. Gt-BuOH treatment was associated with reduced p-EGFR, TOP2A, and TNF-α levels in MCF-7 cells but not in HFF cells. Docking predicted weaker individual binding affinities for the three constituents than for reference inhibitors; no synergy or multi-target advantage is claimed.

Conclusion: These preliminary findings support further investigation of Gt-BuOH as a source of fatty-acid-derived antiproliferative agents, but bioassay-guided fractionation, additional cell lines, and functional validation are required before any therapeutic claims can be made.

Keywords: Plant Extracts, MCF-7 Cells, Breast Neoplasms, Topoisomerase II Inhibitors, Molecular Docking Simulation, ErbB Receptors.

1. INTRODUCTION

Breast cancer is the most common malignancy in women worldwide and second leading cause of cancer related death, with approximately 2.3 million new cases and 685,000 deaths annually [1]. Hormone-dependent subtypes are especially counterproductive in this context, with the MCF-7 luminal A phenotype exhibiting considerable therapeutic challenges due to acquired drug resistance mechanisms, heterogeneous clinical responses, and off-target toxicities from conventional cytotoxic agents [2]. Although approaches such as early detection and targeted therapies have made substantial progress in these aspects, the molecular heterogeneity of breast cancer remains a major challenge for treatment success, highlighting an urgent need to develop better anticancer agents that are safer, more selective and mechanistically diverse or able to bypass resistance pathways while minimizing systemic toxicity [3]. Conventional platinum-based chemotherapeutics remain fundamental to the treatment of breast cancer; nonetheless, their clinical use is severely limited by dose-limiting toxicities (nephrotoxicity, neurotoxicity, ototoxicity and myelosuppression), as well as intrinsic and acquired

*Address correspondence to this author at the Bilad Alrafidain University, Iraq; E-mail: dryoussef@bauc14.edu.iq

ISSN: 1929-2260 / E-ISSN: 1929-2279/26 © 2026 Neoplasia Research

resistance mechanisms which significantly reduce therapeutic effectiveness [4]. Cisplatin is also unstable in aqueous solutions, requiring careful handling and preparation shortly before use, which can contribute to variable experimental results [5]. However, the narrow therapeutic window of these agents often leads to suboptimal dosing that is insufficient to control tumor growth while their non-selective cytotoxicity causes significant collateral damage to rapidly dividing normal tissues, emphasizing the urgent need for new therapeutic strategies with the ability to preferentially kill malignant cells while preserving host tissue integrity and physiological function [5,6]. Plants have always been an important source of antimicrobial and anticancer agents, with natural products accounting for around 60% of all clinically useful antineoplastic agents in use today (e.g., paclitaxel, vincristine, camptothecin and epipodophyllotoxins) [7]. Plant secondary metabolites are characterized by their unique structural complexity and stereochemical diversity that gives them some key advantages compared with synthetic compounds, such as the ability to target multiple molecular targets simultaneously [8], avoid classical resistance mechanisms, and display a favorable toxicity that often exceeds those of synthetic chemotherapeutics [9]. Although this is an established precedence, most plant species — particularly those from underrepresented genera — have not been assayed for their anticancer activity, constituting a large resource pool of potential lead compounds in the drug discovery/development pipeline [10,11].

Gelasia tomentosa (L.) Zaika, Sukhor. The herbaceous perennial species with lanceolate to ensiform leaves and yellow ray florets, previously classified under Scorzonera tomentosa L (Scorzonera) is currently described within the genus Arctium(Compositae—Asteraceae), in tribe Cichorieae [12], sprawling predominantly from Western Asia [13]. The genus Scorzonera sensu lato have been conventionally utilized as folk medicine by the local people e.g. to treat inflammatory disease, fever and in wound healing processes or to improve digestion [14]; however, systematic studies with regard to phytochemical and pharmacological properties have essentially not been done until now. Phytochemical studies of Scorzonera species have identified various secondary metabolites, including sesquiterpenes, triterpenes, flavonoids, phenolic acids, and fatty-acid derivatives, some with promising biological activities, including cytotoxic activity [15]. antioxidant and anti-inflammatory effects. [16] To date, no extensive study in the literature has examined the anticancer activity of the polar and non-polar fractions of G. tomentosa against breast cancer cell lines; therefore, this study represents a first commitment to conducting.

phytopharmacological characterization of this species. The butanolic extract characterized here by GC-MS is dominated by fatty-acid methyl esters and short-chain organic acid derivatives rather than phenolic compounds. GC-MS without derivatization is poorly suited for detecting polar phenolics, and the chemical profile reported here should not be interpreted as evidence of phenolic enrichment. Long-chain unsaturated fatty acid methyl esters, mainly derived from oleic acid, are chemotaxonomic markers of the Asteraceae family and have also been characterized as having pharmacological properties; indeed, it has been established that these compounds possess anticancer effects mediated through induction of apoptosis [18]. Inhibition of proliferation and regulation of lipid metabolism in neoplastic cells [19]. Furthermore, despite being less relevant to the total quantity, short-chain organic acids and anhydride concentrations can act as synergistic agents with biological activity in additive or supplementary mechanisms, potentially increasing crude plant extracts' therapeutic efficacy [21].

Epidermal growth factor receptor (EGFR) is a receptor tyrosine kinase often overexpressed and constitutively activated in breast cancer cell lines, including MCF-7 cells, and can orchestrate pro-survival signaling cascades that are critical for tumor proliferation (PI3K), angiogenesis, and metastasis with the PI3K/AKT pathway and MAPK/ERK pathways; therefore, it is a well-established clinically actionable therapeutic target. Phosphorylation of EGFR at Tyr1068 is a marker of receptor activation, and reduced p-EGFR levels have been associated with decreased cell proliferation and increased apoptosis in breast cancer models [22]. Topoisomerase IIα (TOP2A) is a nuclear enzyme that relieves DNA supercoils and catenanes arising from replication and transcription, and its inhibition generates irreversible double-stranded DNA breaks that lead to apoptosis, making it a clinically validated target for anticancer therapy [23]. Nevertheless, quantification of overall TOP2A protein level with ELISA is not directly reflective of enzymatic activity; functional assays (i.e., DNA relaxation or decatenation assays) would be necessary to verify whether TOP2A catalytic activity was inhibited [24]. Tumor necrosis factor-alpha (TNF-α), a pleiotropic pro-inflammatory cytokine with both tumor-promoting inflammatory signaling and important roles in normal

immune homeostasis, is an attractive therapeutic target that can be selectively modulated within cancer cells without interfering with physiological immune function [25]. Importantly, measurement of intracellular TNF-α levels will not include the secreted fraction, which is also important but would mediate paracrine effects in the tumor microenvironment.

Molecular docking is of key computational technique; it has become a pivotal tool for predicting binding conformations, interaction energies, and affinity profiles between small-molecule ligands and their protein targets, with the goal of generating hypotheses about the molecular mechanisms underlying biological activities [26]. Docking algorithms like AutoDock Vina facilitate the systematic screening of phytoconstituents against several therapeutic targets, offering important structural insights into hydrogen-bonding networks, hydrophobic interactions, and electrostatic complementarity involved in ligand-receptor interaction in silico [27]. Combined with experimental strategies such as cytotoxicity assays and enzyme-linked immunosorbent assays, molecular docking supports hypothesis-generating mechanistic inference of aligning predicted binding affinities with experimental effects, providing additional validation of computational predictions and increasing the overall translational relevance of findings [28].

In contrast to the established ethnopharmacological relevance of Scorzonera species, a systematic screening of Gelasia tomentosa against breast cancer cell lines has so far not been conducted in the literature, marking a substantial research river this study aims to bridge. Thus, the present study aims at a preliminary *in vitro* assessment of cytotoxicity, selectivity and mechanism by which G. tomentosa butanolic extract (Gt-BuOH) acts against MCF-7 breast cancer cells using non-malignant HFF fibroblasts as control along with GC-MS profiling, ELISA-based biomarker quantification and molecular docking simulations to profile phytochemical composition and validate mechanistically-derived hypotheses for anticancer activity through molecular modeling.

2. MATERIALS AND METHODS

2.1. Plant Collection and Authentication

Gelasia tomentosa (L.) Zaika, Sukhor. & N. Kilian (formerly Scorzonera tomentosa L.; family Asteraceae, tribe Cichorieae) was collected in full bloom on May 22, 2025, from Zinya Stopy Mountain, west of Lerre Village, Sherwan Mezn sub-district, Merge Sor, Erbil, Kurdistan Region, Iraq (1674 m altitude). Dr. Ali Mala Khedir Galalay (Salahaddin University, College of Agricultural Engineering Sciences, Department of Field Crops and Medicinal Plants) confirmed the taxonomic identification. Voucher specimens were deposited at the university herbarium (GT-2025-001). All collections were performed under appropriate local authority permits. The aerial parts were collected, washed with distilled water, dried in the dark at room temperature (25 ± 2°C) for two weeks, and powdered using an electric mill. The powdered material was sealed in impermeable vessels and stored in the dark and dry until use.

2.2. Plant Extract Preparation and Drug Preparation

The preparation of the butanolic fraction of Gelasia tomentosa (Gt-BuOH) was carried out using a sequential extraction method with different solvents, followed by a partitioning process. The aerial parts (650 g air-dried powder) were extracted with petroleum ether (w/v 1:10, 2 L, batch time: 24 hours, room temperature with occasional stirring) for the removal of chlorophylls and other lipophilic contaminants. The Soxhlet extraction was continued until the extraction solvent became clear using 90% ethanol (2.5 L, 8 cycles, ca. 8 hours) on defatted plant material. Extraction endpoint was defined as when the solvent became colorless (approx 8 hours).

All extracts were mixed together, dried under reduced pressure at 40°C using a rotary evaporator to yield a crude dry extract of ethanolic extracts. This dried extract was then dissolved in 200 mL of distilled water (pH 3.5 (adjusted with 1N HCl for maximally extracting phenolic acid) and partitioned three times with the use of a separatory funnel by adding 200 mL n-hexane to the aqueous layer, discarding each time the separated upper n-hexane layers in order to eliminate non-polar compounds. The residual aqueous phase was subsequently neutralised to pH 7.0 using 1N NaOH, and extracted three times with 200 mL of n-butanol. The butanol fractions were pooled and dried using a rotary evaporator (Sigma, Germany). The resulting dry powder was stored at −20°C in airtight containers, protected from light and humidity, until use. The extraction yield is expressed as a percentage of the initial dry plant weight [22]. It yielded 88.4 g, equivalent to 13.6% w/w [29].

2.3. Lyophilization of the Butanolic Extract

The butanolic fraction was lyophilized (freeze-dried) after rotary evaporation to attain a stable dry extract for long-term storage and further biological assays. The

concentrated extract was placed in sterile round-bottom flasks (25% v/v), frozen at −80°C for 24 h, and lyophilized (Christ Alpha 1-4 LD plus, Germany) at −55°C under vacuum (0.1 mbar) for 48–72 h until constant weight was reached. The lyophilized powder was scraped, weighed, and stored in dry, dark containers at −20°C until needed. Lyophilization removes residual water and organic solvents without compromising heat-labile phytoconstituents, retaining the bioactivity of the extract [30].

2.4. Gas Chromatography-Mass Spectrometry (GC-MS) Analysis

Chemical composition of lyophilized Gt-BuOH was analyzed using a GC-MS system [Shimadzu, Japan; analysis performed by Metabolon, Inc.] consisting of a GC-2010 gas chromatograph coupled to a GC-MS-QP2010 Plus mass spectrometer. Separation was conducted on a DB-5MS (30 m × 0.25 mm I.D., stationary phase: 5% phenyl-95% dimethylpolysiloxane, film thickness = 0.25 µm) fused silica capillary column. Data were collected by using helium at a constant flow rate of 1.0 mL/min as the carrier gas. The injection port temperature was 280°C; the injection mode was split, with a split ratio of 10:1. The injected volume was 1 µL [31].

The temperature program for the column oven was as follows: 80°C (2 minutes), ramp to 300°C at 10°C/min; hold: 300°C (6 min). Final run time was 30 minutes. The mass spectrometer was operated in EI mode (70 eV) with an ion source temperature of 200 °C and an interface temperature of 250 °C; the solvent cut time was 2.00 minutes. Detection was performed in full scan mode over a mass range of m/z 40–800 at a scan speed of 1666 amu/s [32].

The mass spectra obtained were compared with the NIST20s.lib and NIST20-1.lib spectral libraries to identify possible compounds, with a minimum similarity index (SI) of 70%. Retention indices (RI) were calculated from a C8–C40 linear n-alkane series, and identities were considered confirmed if both the mass spectral match and retention index values matched published literature listings (±10 RI units) [33].

2.5. Cytotoxic Study

2.5.1. Sample Preparation

Lyophilized Gt-BuOH was dissolved in dimethyl sulfoxide (DMSO) to obtain a stock solution of 100 mg/mL stock solution, which was diluted in Minimum Essential Medium (MEM) to final working concentrations of 0.1–1000 µg/mL for cytotoxicity assays. The DMSO concentration never exceeded 0.1% (v/v) in any treatment condition, and vehicle controls (0.1% DMSO) were included in each experiment.

Cisplatin, used as a positive control, was purchased as an active ingredient from Samarra Drug Industries (Iraq). A fresh stock solution of cisplatin was prepared in sterile phosphate-buffered saline (PBS) at 1 mg/mL and diluted in MEM to matching tested ranges (0.1–1000 µg/mL) for comparative evaluation of cytotoxicity. Because cisplatin is unstable in aqueous solution [34], solutions were protected from light and used within 4 h of preparation. All stock solutions were filter-sterilized through 0.22 µm syringe filters before use.

2.5.2. Cell Culture Models and Maintenance

Two cell lines were used: the human breast adenocarcinoma-derived MCF-7 cell line (passage 34) and the normal human foreskin fibroblast (HFF) cell line (passage 22), both kindly provided by the Tissue Culture Unit at the Iraqi Center for Cancer and Medical Genetics Research, Al-Mustansiriyah University. Cell line authentication was verified by STR profiling (last tested within 6 months of use). Cells were cultured in MEM medium (US Biological, USA) supplemented with 10% (v/v) fetal bovine serum (FBS) from Capricorn Scientific (Germany), penicillin 100 IU/mL, and streptomycin 100 µg/mL to prevent bacterial contamination. Mycoplasma contamination was routinely assessed by PCR. [35].

2.5.3. Cell Viability and Cytotoxicity Assay (MTT Assay)

Preliminary experiments established a linear correlation between cell number and MTT reduction over 72 h, and a seeding density of 1×10^4 cells/well in 96-well plates was selected (linear range 0.5×10^4 to 2.5×10^4 cells/well; $R^2 > 0.98$ for both cell lines).

The MTT colorimetric assay was used to determine the cytotoxicity of cisplatin (positive control) and the Lyophilized Gelasia tomentosa butanolic extract (Gt-BuOH), which tests the enzymatic reduction of tetrazolium salt MTT (3-(4,5-dimethylthiazol-2-yl)-2,5-diphenyltetrazolium bromide) by metabolically active cells into insoluble purple formazan crystals in a reaction mainly mediated by mitochondrial dehydrogenase enzymes. Adenosine triphosphate (ATP) assay This method consistently serves as a quantitative measurement of cell viability since the amount of formazan produced directly correlates with

the number of viable cells. Cells were plated onto 96-well microplates at a density of 1 × 10^4 cells per well and incubated in a humidified atmosphere containing 5% CO2 at 37°C for d24 hrs for cell adhesion. The medium was then replaced with Gt-BuOH extract (0.1, 1, 10, 100 and 1000 µg/mL) or cisplatin (0.1, 1, 10, 100 and doubles the concentration of extracts per mL). Untreated control wells received only vehicle (0.1% DMSO in culture medium for extract; PBS for cisplatin). The experimental setup was performed using six technical replicate wells per condition for each of the three independent experiments (biological replicates, n = 3) [36,37].

After incubation times of 24 h and 72 h, each well was supplemented with 20 µL (5 mg/mL) MTT diluted in PBS (pH = 7.4) and incubated for more 4 h at 37 °C in the dark. Afterward, the culture medium was gently removed, and 100µL of DMSO (containing 5% 1N HCl to improve solubilization) was added for dissolving the formazan grains. Plates were incubated at room temperature for 15minutes with gentle shaking. The absorbances were read at 570 nm with background reading at 690 nm using a microplate reader (BioTek, USA). Cell viability percentage was determined according to the following formula [38].

% Cell Viability = *OD of treated wells/OD of control wells* x 100 [39]

The percentage of growth inhibition was calculated as:

Growth inhibition *% = (OD of control wells – OD of treated wells)/OD of control wells* x 100% [18]

The half-maximal inhibitory concentration (IC_{50}), defined as the drug concentration that produces a 50% reduction in cell viability, was computed using GraphPad Prism software (version 9.5.0, build 750) by fitting dose-response curves with nonlinear regression (four-parameter logistic model). The IC_{50} values of the extract were compared with those of cisplatin to evaluate relative potency.

2.5.4. Cytotoxicity Comparison Across Cell Lines and Treatments

To evaluate the selectivity of Gt-BuOH as a potential anticancer agent and to compare it with an established chemotherapeutic agent, MCF7 cancer cells were exposed alongside HFF normal cells at consistent concentration ranges (0.1–1000 µg/mL) and incubation times (24 and 72 hours). In both cell lines, the cytotoxicity of the extracts was directly compared against cisplatin. For each cell line and treatment, IC_{50} values were derived based on the percentage of growth inhibition.

2.6. Evaluation of the Selective Toxicity Index

The SI index was used to examine and compare the cytotoxic selectivity of Gt-BuOH in relation to normal cells and the overall selectivity with respect to cisplatin (D1/C) [2, 21]. It allowed us to quantify preferential cytotoxicity against tumor cells after 24 or 72 hours of incubation time. Growth curve analyses determined IC_{50} values against MCF7 and HFF cells at time, allowing for calculation of the selective cytotoxicity index from the extract or cisplatin by mathematical expression, as follows [41].

$$\textbf{Selective Toxicity Index (SI)} = \frac{IC_{50}\ of\ normal\ cell\ lines\ (HFF)}{IC_{50}\ of\ cancer\ cell\ lines\ (MCF7)}$$

Higher SI scores are indicative of superior drug action on tumor cells vs normal cells, and higher values indicate a greater therapeutic window. The extract SI values were compared to those of cisplatin, and the agent that was superior in cancer cell selectivity was ascertained.

2.7 Enzyme-Linked Immunosorbent Assay (ELISA)

2.7.1 Sample Preparation

MCF-7 and HFF cells (2 × 10^5 cells/well in 6-well plates) were incubated with Gt-BuOH at its IC_{50} against MCF-7 cells (431.8 µg/mL; 72 h). Cisplatin was tested at 112 µg/mL (its IC_{50} against HFF cells) because it did not achieve 50% inhibition against MCF-7 cells within the tested concentration range; this concentration difference must be considered when interpreting comparative data, and cisplatin results are presented for reference only. Untreated controls for both cell lines received 0.1% DMSO. After incubation, cells from each cell line were independently washed with PBS, lysed with RIPA buffer [50 mM Tris-HCl (pH 7.4), 150 mM NaCl, 1% NP-40, 0.5% sodium deoxycholate, 0.1% SDS, containing 1× protease inhibitor cocktail (cOmplete, Roche) and 1× phosphatase inhibitor cocktail (PhosSTOP, Roche)], and centrifuged (14,000 × g, 15 min, 4°C). Supernatants from cancer and normal cells were stored separately at −80°C. Total protein was quantified by the BCA assay [42].

2.7.2. p-EGFR ELISA

p-EGFR (Tyr1068) levels were measured in lysates from MCF-7 and HFF cells using a commercial

sandwich ELISA kit (R&D Systems, USA, Catalog # DYC1095). Lysates (50 µg protein) from each cell line were added to 96-well plates pre-coated with anti-EGFR antibody, incubated (2 h, RT), washed, then incubated with HRP-conjugated detection antibody (1 h, RT). After washing, TMB substrate was added (15 min, dark), and the reaction was stopped with H_2SO_4. Absorbance was read at 450/570 nm. p-EGFR concentrations were interpolated from a standard curve with $R^2 > 0.98$ (range: 15.6-1000 pg/mL, LOD: 3.9 pg/mL, LOQ: 15.6 pg/mL) and expressed as pg/mg total protein [43].

2.7.3. TOP2A ELISA

Total TOP2A protein was quantified in both MCF-7 and HFF cell lysates using a commercial ELISA kit (MyBioSource, USA, Catalog # MBS724559). Lysates (50 µg protein) from each cell line were added to anti-TOP2A-coated plates, incubated (2 h, 37°C), washed, then incubated with biotinylated detection antibody (1 h, 37°C), followed by streptavidin-HRP (30 min, 37°C). TMB substrate was added (15 min, dark), stopped with H_2SO_4, and absorbance was read at 450/570 nm. TOP2A concentrations were calculated from a standard curve with $R^2 > 0.99$ (range: 0.156-10 ng/mL, LOD: 0.039 ng/mL, LOQ: 0.156 ng/mL) and expressed as ng/mg total protein [44]. This assay measures total TOP2A protein levels, not TOP2A enzymatic activity. Functional assays (e.g., DNA relaxation or decatenation assays) would be required to confirm inhibition of TOP2A catalytic function.

2.7.4. TNF-α ELISA

TNF-α levels were measured in lysates of MCF-7 and HFF cells using a commercial sandwich ELISA kit (Invitrogen, USA, Catalog # BMS223-4). Lysates (50 µg protein) from each cell line were added to anti-TNF-α-coated plates, incubated (2 h, RT), washed, and incubated with HRP-conjugated detection antibody (1 h, RT). After washing, TMB substrate was added (15 min in the dark), stopped with H_2SO_4, and absorbance was read at 450/570 nm. TNF-α concentrations were interpolated from a standard curve with $R^2 > 0.99$ (range: 7.8-500 pg/mL, LOD: 2.0 pg/mL, LOQ: 7.8 pg/mL) and expressed as pg/mg total protein of cell lysates [45]. It is important to note that intracellular TNF-α levels represent the stored/protein pool rather than the secreted cytokine that mediates paracrine signaling; measurement of secreted TNF-α in culture supernatants would provide complementary information on functional cytokine release.

2.7.5. Data Calculation

Standard curves were used to interpolate absorbance values. Concentrations obtained were normalized to the total protein (ng/mg or pg/mg total protein). The results in p-EGFR were reported as relative levels with respect to untreated controls. For each biological sample, all ELISA assays were performed in duplicate technical replicates with coefficients of variation < 10% across all independent assay data.

2.8. Molecular Docking Study

Molecular docking was performed as a hypothesis-generating exercise to explore potential interactions between the GC-MS-identified Gt-BuOH constituents and three protein targets. These computational results are predictive and do not constitute direct mechanistic proof; experimental validation is required. Cisplatin was not included in docking analysis because it is a platinum-based inorganic compound whose mechanism of action (DNA crosslinking) differs fundamentally from that of the organic ligands identified in the plant extract.

2.8.1. Target Selection

Three molecular targets were selected based on their established roles in cancer progression and normal cell survival:

Cancer target 1: Epidermal Growth Factor Receptor (EGFR): A receptor tyrosine kinase frequently overexpressed and mutated in breast cancer, including MCF7 cells [46]. Inhibition of EGFR suppresses tumor proliferation and survival. The three-dimensional structure of the EGFR kinase domain was retrieved from the Protein Data Bank (PDB ID: 1M17).in its active conformation (as determined by the presence of phosphorylated tyrosine residues in the activation loop).

Cancer target 2: Topoisomerase IIα (TOP2A): An essential enzyme that resolves DNA supercoils during replication and transcription [47]. TOP2A is a validated anticancer target; its inhibition induces irreversible DNA double-strand breaks, leading to apoptosis in rapidly dividing cancer cells. The crystal structure of human TOP2A was obtained from the PDB (ID: 5GWK).

Additional target: Tumor Necrosis Factor-alpha (TNF-α) - A pro-inflammatory cytokine involved in immune function and cancer-related inflammation [48]. This target was included to assess potential off-target

interactions, given that TNF-α is not a direct cell-viability target but rather a secreted cytokine with complex roles in cancer biology. The structure of TNF-α was retrieved from the PDB (ID: 2AZ5).

2.8.2. Ligand and Protein Preparation

The three-dimensional structures of the selected ligands (based on GC-MS constituent analysis of the Lyophilized Gt-BuOH) were constructed in ChemDraw (CambridgeSoft, USA) and optimized to their lowest-energy conformations using Chem3D with the MM2 force field. The prepared ligands were saved in PDB format.

Protein structures (PDB: 1M17, 5GWK, and 2AZ5) were downloaded from the Protein Data Bank. Water molecules and non-interacting heteroatoms were removed using PyMOL (version 2.5). Hydrogen atoms were added, and Gasteiger charges were computed using AutoDock Tools (version 1.5.7). The protein structures were then converted to PDBQT format, which includes atomic partial charges and solvation parameters [49].

2.8.3. Docking Protocol

Prior to docking the Gt-BuOH compounds, the docking protocol was validated by redocking the co-crystallized ligands (where available). For EGFR (PDB: 1M17), erlotinib was redocked to its binding site; for TOP2A (PDB: 5GWK), the co-crystallized inhibitor was redocked; for TNF-α (PDB: 2AZ5), no co-crystallized small-molecule ligand is available, so the protocol was validated based on literature-reported binding sites. The RMSD between the docked pose and the crystallographic pose of the co-crystallized ligand was calculated, and the protocol was considered valid if RMSD was less than 2.0 Å. For EGFR, the RMSD was 1.2 Å; for TOP2A, the RMSD was 1.5 Å.

Molecular docking simulations were conducted using AutoDock Vina (version 1.1.2). A grid box was centered on the known active site of each target protein, based on co-crystallized ligand coordinates from the PDB. The grid box center coordinates were: EGFR (1M17): x = 25.342, y = 27.148, z = 30.678; TOP2A (5GWK): x = 37.892, y = 21.456, z = 28.934; TNF-α (2AZ5): x = 12.567, y = 8.234, z = 15.678. The grid box dimensions were set to 30 Å × 30 Å × 30 Å with a grid spacing of 1.0 Å to adequately cover the binding pocket. Docking was performed with the following parameters: exhaustiveness = 50 (increased from default 20 to improve conformational sampling), Num modes = 9, and energy range = 4. For each ligand-target pair, nine docking poses were generated and ranked according to their binding affinity (kcal/mol). The pose with the lowest binding energy and most favorable interaction geometry was selected for further analysis.

Inhibition of the targets was also validated by docking known inhibitors: erlotinib for EGFR, etoposide for TOP2A, and curcumin for TNF-α. The use of etoposide as a TOP2A reference has mechanistic limitations because etoposide is a DNA-intercalating TOP2A poison rather than a direct catalytic inhibitor; this limitation is acknowledged in the Discussion. For TNF-α, FDA-approved direct inhibitors are biologic macromolecules (e.g., infliximab, adalimumab) whose large molecular weight (~150 kDa) makes them incompatible with standard small-molecule docking protocols utilizing AutoDock Vina; curcumin, a well-characterized natural polyphenol with reported direct binding to TNF-α, was therefore used as a reference [50]. The root mean square deviation (RMSD) between the docked and crystallographic pose of the reference ligand was determined, and RMSD values <2.0 Å were accepted as reliable [52,53].

2.8.4. Analysis of Docking Interactions

Visualization and analysis of the resulting ligand-protein complexes were performed using BIOVIA Discovery Studio Visualizer version 2021 and UCSF Chimera version 1.15. Types of interactions were then detected and encoded as follows: standard (or conventional) hydrogen bonds, carbon-hydrogen bonds, hydrophobic interactions (in the form of pi-alkyl, alkyl, pi-pi stacked, and pi-pi T-shaped), electrostatic ones (pi-cation and pi-anion), and van der Waals contact types.

The docking scores of each ligand-target pair were compared with the corresponding scores for reference inhibitors to assess the relative predicted binding affinity of Gt-BuOH constituents. In silico predicted interactions generally favor compounds with a lower (more negative) binding energy. These comparisons are hypothesis-generating only and do not constitute evidence of pharmacological synergy or multi-target advantage.

2.9. Morphological Evaluation

After 72 h of treatment, morphological alterations in MCF-7 and HFF cells were evaluated under a phase-contrast microscope (Nikon Eclipse TS100, Japan) at ×200 magnification. Digital images were taken and analyzed for distinguishing features of apoptosis such

as cell shrinkage, membrane bubbling, detachment from the attachment surface, and rounded floating cells. Morphological controls included untreated cells, and a positive control for apoptosis was established by treating cells with cisplatin.

2.10. Statistical Analysis

This study employed rigorous experimental protocols, including multiple biological and technical replicates, to ensure the reliability of the data. All MTT assays were performed in three independent biological replicates (six technical replicates per concentration). Cytotoxicity data are expressed as mean ± standard deviation (SD).

Two-way analysis of variance (ANOVA) was used to assess differences across drug concentrations, cell lines, treatment types (extract vs. cisplatin), and treatment durations, followed by Tukey's HSD post hoc tests for specific group comparisons when significant effects were identified. For comparisons between two groups only (e.g., Gt-BuOH vs. cisplatin at a single concentration), independent t-tests were used with Bonferroni correction for multiple comparisons to control the family-wise error rate. Statistical significance was set at $p < 0.05$. Data were interpreted using a letter-coding system, in which different letters denote statistically significant differences ($p < 0.05$) based on homogeneous subsets from Tukey's HSD test. IC_{50} values were calculated using GraphPad Prism software (version 9.5.0, build 750) by fitting a four-parameter logistic (4PL) nonlinear regression model to the dose-response data. Assumptions of normality (Shapiro-Wilk test) and homogeneity of variances (Levene's test) were checked before applying parametric tests. Analyses were conducted using IBM SPSS Statistics (version 20) [56].

Post-hoc tests were performed (Tukey) and results coded as letters for easy interpretation. Values within each column with different letter are significantly different ($p < 0.05$) while values of same letters means that there is no statically significant difference ($p \geq 0.05$). This makes it easy to visually compare multiple groups and summarise the statistical results into a table. [57].

3. RESULTS

3.1. Extraction Ratio

A stepwise solvent fractionation method was used to evaluate the extraction efficiency of aerial parts of Gelasia tomentosa. Petroleum ether was used to delipidate about 650 g of pulverized plant tissue, which was then Soxhlet-extracted with 90% ethanol before being fractionated between n-hexane and n-butanol. The butanol fraction was concentrated by rotary evaporation, frozen at -80 °C for 24 h and lyophilized at −55 °C under a vacuum of 0.1 mbar for 48 h to preserve thermolabile compounds. From the lyophilized powder, 88.4 g of crude extract was obtained, giving an extraction yield of 13.6% (w/w), relative to dry biomass used in the process up till month of October 2023.

3.2. Cytotoxic assay

3.2.1. Cytotoxic Efficacy of the Gt-BuOH

To determine the cytotoxic activity of Gt-BuOH against MCF-7 breast cancer cells and normal HFF cells, we used the MTT assay at different concentrations (0.1–1000 µg/mL) for 24 and 72 h. MCF-7 cell proliferation inhibition by Gt-BuOH was found to be concentration-dependent, ranging from 2.0 ± 0.2% at 0.1 µg/mL to as high as ~59.0 ± 0.3% at 1000 µg/mL after 24 h of cultivation time. The cytotoxic effects were markedly time-dependent, with 75.0 ± 0.3% inhibition observed at the maximum concentration after 72 h of exposure. IC_{50} values of MCF-7 cells were 785.7 µg/mL at 24 h and 431.8 µg/mL at 72 h, indicating a significant increase in potency with longer exposure. By comparison, Gt-BuOH showed substantially lower toxicity toward normal HFF cells (inhibition of 7.0 ± 0.4% to 10.0 ± 0.7% at 24 h and 14.0 ± 0.7% to 16.0 ± 0.3% at 72 h at the respective concentrations). At both time points, the IC_{50} values for HFF cells were >1000 µg/mL, suggesting a good safety profile (Tables **1** and **2**).

3.2.2. Cytotoxicity of Cisplatin

The cytotoxic activity of cisplatin, used as a positive control, was evaluated against the MCF-7 and HFF cell lines under identical experimental conditions. Cisplatin exhibited moderate cytotoxicity against MCF-7 cells, with inhibition increasing from 10.0 ± 1.3% at 0.1 µg/mL to 41.0 ± 3.1% at 1000 µg/mL after 24 hours. However, at 72 hours, a paradoxical decrease in inhibition was observed across all concentrations, with values declining from 5.0 ± 1.5% at 0.1 µg/mL to 32.0 ± 3.1% at 1000 µg/mL. Consequently, the IC_{50} values for MCF-7 cells exceeded 1000 µg/mL at both time points, indicating relatively low potency under the tested conditions. Importantly, cisplatin exhibited substantial toxicity toward normal HFF cells, with inhibition increasing from 2.0 ± 1.5% at 0.1 µg/mL to 48.0 ± 4.1% at 1000 µg/mL after 24 hours, and reaching 63.0 ± 4.8% at 72 hours. The IC_{50} for HFF cells was >1000

Table 1: Cytotoxic Activity of Gt-BuOH Against MCF7 and HFF Cell Lines at 24 and 72 Hours

Con (µg/ml)	Cellular proliferation inhibition (mean ± SD)					
	MCF7 cell line			HFF cell line		
	24 hr.	72 hr.	*P*- value	24 hr.	72 hr.	*P*- value
0.1	D 2 ± 0.2	D 12 ± 0.3	< 0.001*	C 7 ± 0.4	A 14 ± 0.7	0.002*
1	C 7 ± 0.8	C 16 ± 0.7	< 0.001*	BC 8 ± 0.4	A 15 ± 0.3	0.001*
10	C 10 ± 1.1	C 18 ± 0.8	< 0.001*	BC 8 ± 0.8	A 15 ± 0.5	0.001*
100	B 17.0 ± 0.7	B 31 ± 0.9	< 0.001*	AB 9 ± 0.2	A 16 ± 0.9	0.002*
1000	A 59.0 ± 0.3	A 75 ± 0.3	< 0.001*	A 10 ± 0.7	A 16 ± 0.3	0.001*
IC 50	785.7 µg/ml	431.8 µg/ml	-	>1000 µg/ml	>1000 µg/ml	-
LSD value	3.08	2.85	-	1.96	2.04	-

Data are expressed as mean ± standard deviation (SD) of cellular proliferation inhibition (%). Different letters within each column denote statistically significant differences ($p < 0.05$) among concentrations for each cell line and time point, as identified by two-way ANOVA followed by Tukey's post-hoc test. P-values for 24 vs 72 h comparison were obtained by paired t-test. Statistically significant ($P^* < 0.05$). IC_{50} values were derived from dose-response curves.

Table 2: Comparison of the Cytotoxic Effects of the Gt-BuOH on MCF7 and HFF Cells

Con (µg/ml)	Cellular proliferation inhibition (mean ± SD)					
	24 hr.			72 hr.		
	MCF7 cell line	HFF cell line	*P*- value	MCF7 cell line	HFF cell line	*P*- value
0.1	2 ± 0.2	7 ± 0.4	< 0.001*	12 ± 0.3	14 ± 0.7	0.005*
1	7 ± 0.8	8 ± 0.4	0.08	16 ± 0.7	15 ± 0.3	0.06
10	10 ± 1.1	8 ± 0.8	0.08	18 ± 0.8	15 ± 0.5	0.003*
100	17.0 ± 0.7	9 ± 0.2	< 0.001*	31 ± 0.9	16 ± 0.9	< 0.001*
1000	59.0 ± 0.3	10 ± 0.7	< 0.001*	75 ± 0.3	16 ± 0.3	< 0.001*
IC 50	785.7 µg/ml	>1000 µg/ml		431.8 µg/ml	>1000 µg/ml	
LSD value						

Data are expressed as mean ± standard deviation (SD) of cellular proliferation inhibition (%). P-values were obtained by independent t-test with Bonferroni correction for MCF-7 vs HFF comparison at each concentration and time point. IC_{50} values were derived from dose-response curves. * = statistically significant ($p < 0.05$).

µg/mL at 24 hours but decreased to 112 µg/mL at 72 hours, indicating enhanced toxicity to normal cells over time Table **3**.

3.2.3. Comparison of cytotoxicity between Gt-BuOH and cisplatin

A direct comparison between Gt-BuOH and cisplatin revealed distinct cytotoxicity profiles against MCF7 cells. At 24 hours, cisplatin exhibited significantly higher inhibition than Gt-BuOH across all concentrations ($P < 0.01$), with inhibition values of 10.0–41.0% compared to 2.0–59.0% for Gt-BuOH. Notably, at 1000 µ g/mL, Gt-BuOH (59.0 ± 0.3%) surpassed cisplatin (41.0 ± 3.1%; $P < 0.001$). At 72 hours, a marked shift in potency was observed; Gt-BuOH demonstrated significantly higher inhibition than cisplatin at 0.1 µg/mL (12.0 ± 0.3% vs 5.0 ± 1.5%; P = 0.001), 1 µg/mL (16.0 ± 0.7% vs 9.0 ± 1.3%; P = 0.001), and 1000 µg/mL (75.0 ± 0.3% vs 32.0 ± 3.1%; $P < 0.001$). At 100 µg/mL, both agents exhibited comparable activity (31.0 ± 0.9% vs 27.0 ± 3.0%; P = 0.091, NS). IC_{50} values provided additional confirmation of these results; Gt-BuOH decreased significantly from 785.7 µg/mL at 24 hr to 431.8 µg/mL at 72 hr suggesting an increase in activity with time (≤50% inhibition). In contrast, cisplatin had an IC_{50} > 1000 µg/mL at both time points for MCF7 cells, indicating a lack of effectiveness against MCF7 under these conditions. This indicates that while cisplatin is more acutely cytotoxic at early time points, Gt-BuOH activity increases and persists with prolonged exposure under the conditions evaluated. Indeed, the surprisingly low potency of cisplatin needs investigation Table **4**.

3.2.4. Selective toxicity assay

The cytotoxicity index (SI) was determined to measure the selective toxicity of Gt-BuOH and cisplatin against MCF-7 cancer cells compared to normal HFF cells. Interestingly, at 72 h after drug incubation, the SI value of Gt-BuOH was >1.27 at 24 h but increased

Table 3: Cytotoxic Activity of Cisplatin Against MCF7 and HFF Cell Lines at 24 and 72 Hours

Con (µg/ml)	Cellular proliferation inhibition (mean ± SD)					
	MCF7 cell line			HFF cell line		
	24 hr.	72 hr.	*P*- value	24 hr.	72 hr.	*P*- value
0.1	D 10 ± 1.3	E 5 ± 1.5	0.049*	E 2 ± 1.5	E 13.0 ± 1.5	0.002*
1	C 13 ± 2.0	D 9 ± 1.3	0.04*	D 10 ± 1.5	D 19.0 ± 1.5	0.003*
10	B 20 ± 2.1	C 13 ± 2.0	0.02*	C 24.0 ± 1.9	C 37.0 ± 3.9	0.01*
100	A 39 ± 2.6	B 27 ± 3.0	0.01*	B 37.0 ± 3.7	B 49.0 ± 4.1	0.02*
1000	A 41 ± 3.1	A 32 ± 3.1	0.03*	A 48.0 ± 4.1	A 63.0 ± 4.8	0.01*
IC 50	>1000 µg/ml	>1000 µg/ml	-	>1000 µg/ml	112 µg/ml	-
LSD value	2.74	2.77	-	3.30	4.11	-

Data are expressed as mean ± standard deviation (SD) of cellular proliferation inhibition (%). Different letters within each column denote statistically significant differences ($p < 0.05$) among concentrations for each cell line and time point, as identified by two-way ANOVA followed by Tukey's post-hoc test. P-values for 24 vs 72 h comparison were obtained by independent t-test. IC_{50} values exceeding the highest tested concentration (1000 µg/mL) are denoted as ">1000 µg/mL". * = statistically significant ($p < 0.05$).

Table 4: Comparative Cytotoxicity of Gt-BuOH and Cisplatin Against MCF7 Cells at 24 and 72 Hours

Concentration (µg/ml)	Cellular proliferation inhibition (mean ± SD)					
	24 hr.			72 hr.		
	Extract	cisplatin	*P*- value	Extract	cisplatin	*P*- value
0.1	D 2 ± 0.2	D 10 ± 1.3	< 0.001*	D 12 ± 0.3	E 5 ± 1.5	0.001*
1	C 7 ± 0.8	C 13 ± 2.0	0.008*	C 16 ± 0.7	D 9 ± 1.3	0.001*
10	C 10 ± 1.1	B 20 ± 2.1	0.002*	C 18 ± 0.8	C 13 ± 2.0	0.016*
100	B 17.0 ± 0.7	A 39 ± 2.6	< 0.001*	B 31 ± 0.9	B 27 ± 3.0	0.091
1000	A 59.0 ± 0.3	A 41 ± 3.1	< 0.001*	A 75 ± 0.3	A 32 ± 3.1	< 0.001*
IC 50	785.7 µg/ml	>1000 µg/ml	-	431.8 µg/ml	>1000 µg/ml	-
	3.08	2.74	-	2.85	2.77	-

Data are expressed as mean ± standard deviation (SD) of the cell proliferation inhibition rate (%). P-values for comparisons between Gt-BuOH and Cisplatin at each specific concentration and time point were determined using the independent samples t-test with Bonferroni correction. Different letters within a row indicate statistically significant differences ($p < 0.05$) between treatments, based on the independent samples t-test. The symbol NS denotes no statistical significance ($p \geq 0.05$), while the symbol * indicates statistical significance ($p < 0.05$). IC_{50} values exceeding the highest tested concentration (1000 µg/mL) are reported as ">1000 µg/mL".

significantly to >2.32 with extended drug exposure, indicating that prolonged drug exposure time improves cancer cell selectivity and efficacy. The selective reproducibility of this trend with time relates both to a concomitant decrease of IC_{50} against MCF-7 cells (as shown in Table **1**) from 785.7 to 431.8 µg/mL, accompanied by maintenance of an IC_{50} >1000 µg/mL against normal HFF cells at both time points. In sharp contrast, cisplatin had an SI of 1.00 at 24 h (i.e., equal cellular toxicities to both cancer and normal cells). Cisplatin had an SI of <0.11 at 72 h (IC_{50} against HFF = 112 µg/mL; IC_{50} against MCF-7 >1000 µg/mL). These results show that Gt-BuOH has favorable, time-dependent, selective *in vitro* cytotoxicity compared to cisplatin, which was poorly selective and, at longer exposure times, appears more toxic to normal cells. Although the data indicate that cisplatin was unexpectedly toxic to normal cells with little effect on cancer under these conditions, methodological issues must be addressed before firm conclusions can be made (Table **5**).

3.3. Gas Chromatography-Mass Spectrometry (GC-MS) Analysis of Gt-BuOH

A GC-MS analysis was performed on the butanolic extract of Gelasia tomentosa (Gt-BuOH) to characterize its chemical composition and identify putative phytoconstituents responsible for the cytotoxic activity observed in this study. The GC-MS chromatogram (total ion chromatograms, TIC) of the butanolic fraction in shown in Fig.(1), which indicates a severe complex separation parameter with different volatile and semi-volatile compounds.

Table 5: Selective Toxicity Index (SI) of Gt-BuOH and Cisplatin Against MCF7 Cancer Cells and Normal HFF Cells

Treatment	Incubation Time	IC_{50} (MCF7)	IC_{50} (HFF)	Selective Index (SI)
Gt-BuOH	24 hours	785.7	>1000	>1.27
	72 hours	431.8	>1000	>2.32
Cisplatin	24 hours	>1000	>1000	1.00
	72 hours	>1000	112	< 0.11

SI = IC_{50} (HFF) / IC_{50} (MCF7). SI > 1.0 indicates preferential cytotoxicity toward cancer cells; SI < 1.0 indicates greater toxicity to normal cells. IC_{50} values exceeding the highest tested concentration (1000 µg/mL) are denoted as ">1000 µg/mL.

3.3.1. Major Constituents: Fatty Acid Methyl Esters

Analysis established that the butanolic extract mainly consists of unsaturated fatty acid methyl esters, with methyl oleate (9-octadecenoic acid methyl ester) as the principal constituent (Peak 5). The compound was detected at a retention time of about 18.884 min (consistent with an estimated RI of ~2085) and showed the highest area intensity among the signals detected (71.62% normalized area), indicating it is quantitatively dominant in this extract.

Methyl oleate ($C_{19}H_{36}O_2$; MW 296 g/mol) was tentatively identified by comparing its mass spectrum with the NIST20s.lib and NIST20-1.lib spectral libraries, with a similarity index>70%. The identification was confirmed by matching the retention index (RI = 2085) with published values in the literature (RI = 2087 ± 5). The structure is an 18-carbon chain with a cis double bond at the Δ9 position, esterified with methanol. Isomeric octadecenoic acid methyl esters were also detected alongside methyl oleate, suggesting extraction of several unsaturated fatty acid derivatives.

3.3.2. Additional Identified Compounds

Several other constituents were identified at varying concentrations throughout the chromatographic run:

Propanoic anhydride (propionic anhydride; $C_6H_{10}O_3$; MW 130 g/mol) was detected as a minor constituent eluting at a retention time of 17.052 min (RI: 921; Peak 3). The identification was supported by a spectral match with a similarity index of 90% against the NIST20slib database.

1-Pentene (C_5H_{10}; MW 70 g/mol; Peak 1) and 2-methyl-1-butene (C_5H_{10}; MW 70 g/mol; Peak 2) were identified as volatile hydrocarbons eluting early in the chromatogram (RT: 2.834 and 6.173 min, respectively), representing typical plant volatile organic compounds with limited direct pharmacological significance. 4-Methyl-2-hexyne (C_7H_{12}; MW 96 g/mol; Peak 6) was detected as a trace constituent at a retention time of 19.108 min with a similarity index of 83%.

Importantly, the GC-MS profile is dominated by fatty-acid methyl esters and short-chain organic acid derivatives, not phenolic compounds. GC-MS without derivatization is poorly suited for detecting polar phenolics, and the chemical profile reported here should not be interpreted as evidence of phenolic enrichment. The bioactive constituents of Gt-BuOH appear to be fatty-acid derivatives.

3.4. Enzyme-Linked Immunosorbent Assay (ELISA) Analysis of Cellular Biomarkers

The protein levels of three important cellular targets—EGFR phosphorylated at tyrosine 1068, topoisomerase IIα (TOP2A), and TNF-α—were quantified in MCF-7 breast cancer cells and normal HFF cells using ELISA assays to explore associations between treatment and changes in these biomarkers. Gt-BuOH was tested at its IC_{50} against MCF-7 cells (431.8 µg/mL; 72 h), and cisplatin was tested at 112 µg/mL (its IC_{50} against HFF cells). Because cisplatin did not achieve 50% inhibition against MCF-7 cells within the tested concentration range, a direct comparison of biomarker modulation at equi-effective concentrations was not feasible. Cisplatin results are therefore presented for reference only, and the concentration difference must be considered when interpreting comparative data. The merit of these biomarkers arises from their established roles in neoplastic growth, DNA replication, and inflammatory signaling, while they represent the receptor targets tested through the computational docking analysis.

3.4.1. p-EGFR Expression Levels

Exposure of MCF-7 breast cancer cells to Gt-BuOH at its half-maximal inhibitory concentration (431.8 µg/mL) for 72 h was associated with a marked reduction in p-EGFR levels compared with untreated controls (Table **7**). The p-EGFR concentration dropped from 245.6 ± 12.3 pg/mg protein in untreated MCF-7 cells to 98.4 ± 8.7 pg/mg protein after Gt-BuOH exposure ($p < 0.001$), representing a 59.9% reduction. Cisplatin treatment (at 112 µg/mL, its IC_{50} against HFF

Table 6: Phytoconstituents Identified in Gelasia Tomentosa Butanolic Extract (Gt-BuOH) by GC-MS Analysis

Peak No.	R. Time (min)	Compound Name	Molecular Formula	Molecular Weight (g/mol)	Similarity Index (SI %)	Area %
1	2.834	1-Pentene	C_5H_{10}	70	70	11.82
2	6.173	2-Methyl-1-butene	C_5H_{10}	70	69	3.06
3	17.052	Propionic anhydride (Propanoic anhydride)	$C_6H_{10}O_3$	130	90	10.34
4	18.821	Methyl butyrate (Butanoic acid methyl ester)	$C_5H_{10}O_2$	102	92	1.64
5	18.884	Methyl oleate (9-Octadecenoic acid methyl ester)	$C_{19}H_{36}O_2$	296	>90	71.62
6	19.108	4-Methyl-2-hexyne	C_7H_{12}	96	83	1.52

Data are expressed as RT (min) and Area%. The mass spectra of identified compounds were compared to the NIST20 library data. The similarity index (SI) values assess the match between the experimental spectrum and library spectrum, and SI ≥ 70% are accepted as tentative identification results. Retention indices (RI) were matched by comparing published RI values (±10 RI units) and therefore confirmed. The major component was methyl oleate (71.62% area). We analyzed the samples by GC-MS under the following conditions: Column oven temperature programmed from 80°C to 300°C at a rate of 10°C/min; injection temperature set to 280 °C; helium carrier gas flow at 1.46 mL/min; split injection mode (ratio of injected sample vapor: carrier gas = 10:1); mass spectra were acquired in electron impact (EI) ionization mode at an electron energy of 70 eV, scan range m/z 40–800.

Table 7: Comparative Analysis of p-EGFR, TOP2A, and TNF-α Levels in MCF-7 and HFF Cells Following Gt-BuOH and Cisplatin Treatment (72 hours)

Cell Line	Treatment	p-EGFR (pg/mg protein)	% Change	P-value	TOP2A (ng/mg protein)	% Change	P-value	TNF-α (pg/mg protein)	% Change	P-value
MCF-7	Control	245.6 ± 12.3	—	—	18.7 ± 1.4	—	—	156.8 ± 9.4	—	—
	Gt-BuOH	98.4 ± 8.7	59.9%	<0.001*	6.3 ± 0.8	6.3%	<0.001*	72.3 ± 6.8	53.9%	<0.001*
	Cisplatin	189.3 ± 10.5	22.9%	0.012*	12.4 ± 1.1	33.7%	0.004*	118.5 ± 8.2	24.4%	0.008*
HFF	Control	32.4 ± 4.1	—	—	4.2 ± 0.6	—	—	28.6 ± 3.2	—	—
	Gt-BuOH	29.8 ± 3.7	8.0%	0.342	3.9 ± 0.5	7.1%	0.418	26.1 ± 3.5	8.7%	0.372
	Cisplatin	58.7 ± 5.2	1.2%	0.003*	6.8 ± 0.7	61.9%	0.008*	45.3 ± 4.1	58.4%	0.005*

Data are expressed as mean ± SD (n = 3 independent experiments). P-values were determined by one-way ANOVA followed by Tukey's post-hoc test for treatment comparisons within each cell line. *p < 0.05 was considered statistically significant. NS = not significant (p ≥ 0.05). Gt-BuOH treatment was at 431.8 µg/mL (72-hour IC_{50} against MCF-7), and cisplatin treatment was at 112 µg/mL (72-hour IC_{50} against HFF cells). The difference in treatment concentrations should be considered when interpreting comparative data. + indicates increase rather than inhibition.

cells) was associated with a moderate decrease in p-EGFR levels (189.3 ± 10.5 pg/mg protein; p = 0.012 vs. control), corresponding to a 22.9% reduction; however, given the different concentrations used, direct comparison between Gt-BuOH and cisplatin is not valid.

In normal HFF cells, baseline p-EGFR expression was considerably lower (32.4 ± 4.1 pg/mg protein) than in MCF-7 breast cancer cells. Treatment with Gt-BuOH did not significantly alter p-EGFR levels in these non-malignant fibroblasts (29.8 ± 3.7 pg/mg protein; p = 0.342), indicating minimal disruption of physiological EGFR signaling. In contrast, cisplatin exposure (at 112 µg/mL) was associated with increased p-EGFR in HFF cells to 58.7 ± 5.2 pg/mg protein (p = 0.003 vs. control), potentially reflecting a stress-induced compensatory response that may contribute to its off-target toxicity (Table **7**).

3.4.2. TOP2A Expression Levels

TOP2A protein levels in MCF-7 cells were significantly elevated at baseline (18.7 ± 1.4 ng/mg protein) compared to HFF cells (4.2 ± 0.6 ng/mg protein), consistent with the heightened proliferative state of cancer cells (Table **7**). Gt-BuOH treatment reduced TOP2A levels in MCF-7 cells to 6.3 ± 0.8 ng/mg protein (66.3% reduction; p < 0.001). Cisplatin treatment (112 µg/mL) was associated with a more moderate reduction to 12.4 ± 1.1 ng/mg protein (33.7% reduction; p = 0.004); however, direct comparison is limited by the different concentrations used (431.8 µg/mL vs. 112 µg/mL).

In HFF cells, Gt-BuOH did not significantly alter TOP2A expression (3.9 ± 0.5 ng/mg protein; p = 0.418), suggesting selective association with cancer cell DNA replication machinery. Conversely, cisplatin treatment (112 µg/mL) increased TOP2A levels in HFF

cells to 6.8 ± 0.7 ng/mg protein (p = 0.008 vs. control), suggesting a dysregulated stress response that may underlie its toxicity to normal cells (Table **7**). It is emphasized that these measurements reflect total TOP2A protein levels, not enzymatic activity; functional assays would be required to confirm inhibition of TOP2A catalytic function.

3.4.3. TNF-α Expression Levels

TNF-α levels were measured to assess the inflammatory profile of both treated and untreated cells for potential off-target immunomodulatory effects. In MCF-7 cells, Gt-BuOH treatment was associated with a reduction in TNF-α levels from 156.8 ± 9.4 pg/mg protein (control) to 72.3 ± 6.8 pg/mg protein (53.9% reduction; p < 0.001). Cisplatin treatment (112 µg/mL) reduced this to 118.5 ± 8.2 pg/mg protein (24.4% reduction; p = 0.008). The greater reduction observed with Gt-BuOH may reflect the different concentrations used (431.8 µg/mL vs. 112 µg/mL) rather than superior activity.

In HFF cells, Gt-BuOH treatment did not significantly affect TNF-α levels (control: 28.6 ± 3.2 pg/mg protein; Gt-BuOH: 26.1 ± 3.5 pg/mg protein; p = 0.372), suggesting minimal interference with normal cellular immune homeostasis *in vitro*. In comparison, exposure of HFF cells to cisplatin (112 µg/mL) was associated with increased TNF-α production to 45.3 ± 4.1 pg/mg protein (p = 0.005 vs. control), reflecting a pro-inflammatory stress response that may contribute to its cytotoxicity toward non-cancerous cells (Table **7**). Intracellular TNF-α levels represent the stored protein pool rather than secreted cytokine; measurement of secreted TNF-α would provide complementary information.

3.5. Molecular Docking Studies

Molecular docking simulations were performed to explore potential interactions between the three major GC-MS-identified Gt-BuOH constituents (methyl oleate, methyl butyrate, and propanoic anhydride) and three protein targets: EGFR (PDB: 1M17), TOP2A (PDB: 5GWK), and TNF-α (PDB: 2AZ5). The docking protocol was validated by redocking co-crystallized ligands: RMSD values were 1.2 Å for EGFR and 1.5 Å for TOP2A, confirming the reliability of the protocol. For TNF-α, which lacks a co-crystallized small-molecule ligand, the binding site was defined based on literature reports. The analyses employed established computational tools, including AutoDock Tools 1.5.7, BIOVIA Discovery Studio, UCSF Chimera, and AutoDock Vina [57]. Docking scores are presented neutrally as predicted binding affinities and are hypothesis-generating only; they do not constitute evidence of functional inhibition or pharmacological synergy

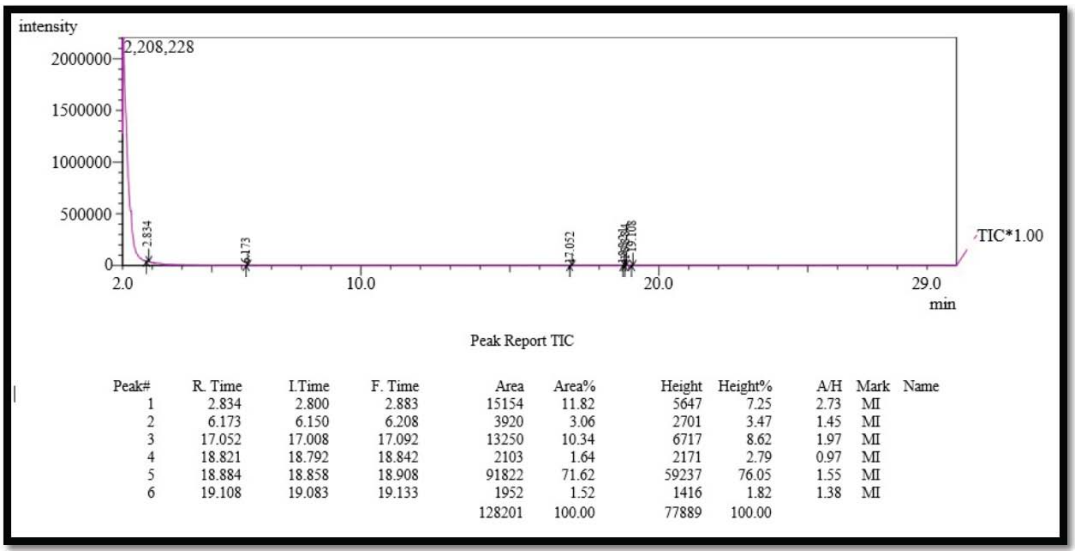
3.5.1. Docking with Epidermal Growth Factor Receptor (EGFR)

The molecular docking study of the active chemical constituents of Gt-BuOH, as identified by GC-MS analysis, was conducted with the human epidermal growth factor receptor (EGFR) kinase domain. The results indicated that Methyl butyrate acid exhibited a docking score of -5.1 kcal/mol with the human EGFR kinase domain. The interaction profile includes two conventional hydrogen bonds with ASP A:831 and LYS A:721 at distances of 2.31 Å and 2.15 Å, respectively. One carbon-hydrogen bond with ASP A:831 at a distance of 2.63 Å. Finally, two alkyl interactions with LYS A:721 and LEU A:764 at 3.92 Å and 4.41 Å, respectively (Figure **2**).

Regarding the molecular docking of oleic acid methyl ester with the human EGFR kinase domain, the docking score was -5.7 kcal/mol. The interaction profile includes seven alkyl hydrogen bonds with two VAL A:702, one residue of LEU A: 820, and two residues of LEU A: 694 at distances of 4.96 Å, 3.78 Å, 5.33 Å, 4.68 Å, 5.39 Å, 4.96 Å, and 4.62 Å, respectively (Figure **2**).

In the molecular docking of propanoic acid anhydride with the human EGFR kinase domain, the docking score was -5.4 kcal/mol. The interaction profile includes two conventional hydrogen bonds with CYS A:751 and ASP A:831 at distances of 2.65 Å and 2.44 Å, respectively (Figure **2**).

For comparison, a molecular docking study was conducted between the human EGFR and erlotinib, a human EGFR inhibitor. [58]. This yielded a docking score of -7.1 kcal/mol. The interaction profile delineates two conventional hydrogen bonds involving LYS A:721 and MET A:769 residues at distances of 2.15 Å and 1.89 Å. Additionally, one carbon-hydrogen bond was identified with GLN A:767 residues at a distance of 3.67 Å. Three pi-anion interactions were observed with three residues from ASP A:831 at distances of 3.73 Å, 3.65 Å, and 4.10 Å, respectively. Furthermore, one pi-pi-stacked interaction involving PHE A:699 at 3.74 Finally, five pi-alkyl interactions were identified with residues PHE A:699, LYS A:721, LEU A:820, and two residues from VAL A:702, at distances of 5.04 Å, 5.07 Å, 5.32 Å,4.84 Å, and 4.11 Å (Figure **2**).



Peak Report TIC

Peak#	R. Time	I.Time	F. Time	Area	Area%	Height	Height%	A/H	Mark	Name
1	2.834	2.800	2.883	15154	11.82	5647	7.25	2.73	MI	
2	6.173	6.150	6.208	3920	3.06	2701	3.47	1.45	MI	
3	17.052	17.008	17.092	13250	10.34	6717	8.62	1.97	MI	
4	18.821	18.792	18.842	2103	1.64	2171	2.79	0.97	MI	
5	18.884	18.858	18.908	91822	71.62	59237	76.05	1.55	MI	
6	19.108	19.083	19.133	1952	1.52	1416	1.82	1.38	MI	
				128201	100.00	77889	100.00			

Figure 1: Total Ion Chromatogram (TIC) of Gt-BuOH Extract Analyzed by Gas Chromatography-Mass Spectrometry (GC-MS). GC-MS analysis of Gt-BuOH extract: Total ion chromatogram (TIC) Chromatogram showing the separation of all volatile compounds in a retention time range between 2.0–29.0 minutes Mass spectra were compared with the NIST20 library to identify peaks. The peak with the highest area (71.62%) was observed at 18.884 min and it belongs to oleic acid methyl ester (9-octadecenoic acid(Z)-methyl ester), a major component of fatty acids. The other major peaks included n-propyl acrylate (2.834 min, 11.82% area) and N-nitrosodimethylamine (17.052 min, 10.34% area). Peaks appeared at 6.173 min, 18.821 min and 19.108 min with lower height (Figure 5A). GC-MS conditions: Column oven temperature ramped from 80°C to 300°C at a rate of 10°C/min; injection temperature was maintained at 280°C; helium as carrier gas with a constant flow rate of approximately 1.46 mL/min and using split injection mode; mass spectra recorded in scan mode (m/z range of detection between 40 and 800).

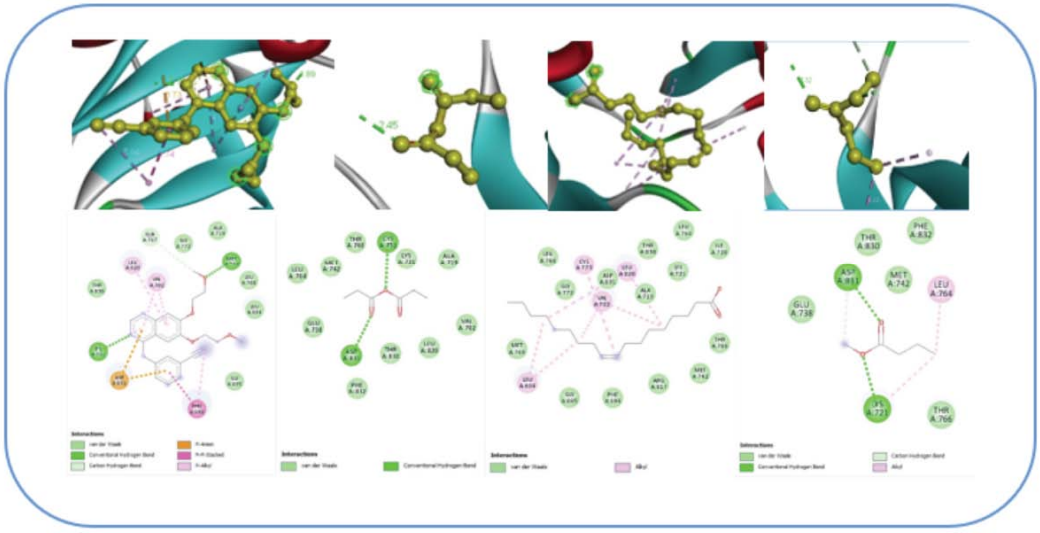


Figure 2: The structural configurations of the human epidermal growth factor receptor (EGFR) binding sites are shown in both two-dimensional (upper image) and three-dimensional (lower image) views, illustrating the binding interactions with the following molecules from right to left (Methyl butyrate acid, oleic acid methyl ester, propanoic acid anhydride, and erlotinib) with the EGFR subunit.

3.5.2. Docking with Topoisomerase IIα (TOP2A)

The molecular docking analysis of the active chemical constituents of Gt-BuOH, as identified by GC-MS, with the Topoisomerase IIα protein revealed that Methyl butyrate acid interacts with the TOP2A protein, yielding a docking score of -5.2 kcal/mol. The interaction profile comprises two conventional hydrogen bonds with the ARG A:727 residue, at distances of 2.37 Å and 2.03 Å. One carbon-hydrogen bond with ILE A:715 at a distance of 3.35 Å. Finally, one pi-sigma bond with the residue of PHE A:1003 at a distance of 3.59 Å (Figure **3**).

Regarding the molecular docking of oleic acid methyl ester with the TOP2A protein, the docking score was -6.3 kcal/mol. The interaction profile comprises

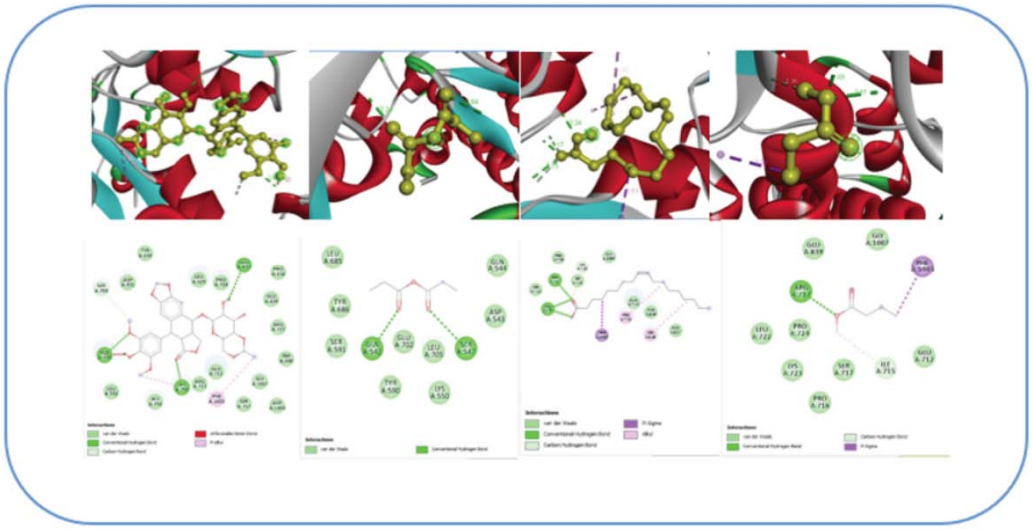


Figure 3: The structural configurations of the Topoisomerase IIα binding sites are shown in both two-dimensional (upper image) and three-dimensional (lower image) views, illustrating the binding interactions with the following molecules from right to left (Methyl butyrate acid, oleic acid methyl ester, propanoic acid anhydride, and etoposide) with the Topoisomerase IIα subunit.

three conventional hydrogen bonds with residues of SER A:717, and two residues of ARG A:727 at distances of 2.74 Å, 2.24 Å, and 2.16 Å, respectively. Two carbon-hydrogen bonds with SER A:717 and SER A:723 at a distance of 3.46 Å and 3.66 Å, respectively; one pi-sigma bond with the residue of PHE A:1003 at a distance of 3.51 Å. and finally two alkyl bonds with the residues of PRO A: 724 and LEU A: 829 at a distance of 4.35 Å and 5.40 Å, respectively (Figure **3**).

In the molecular docking of propanoic acid anhydride to the TOP2A protein, the docking score was -5.5 kcal/mol. The interaction profile includes two conventional hydrogen bonds with GLN A:542 and SER A:547 at distances of 2.24 Å and 2.83 Å, respectively (Figure **3**).

For comparison, a molecular docking study was conducted to assess the interaction between the TOP2A protein and etoposide (a inhibitor of TOP2A). [59]. This yielded a docking score of -8.1 kcal/mol. The interaction profile delineates three conventional hydrogen bonds involving GLN A:544, HIS A:759, and GLU A:837 at distances of 2.47 Å, 1.79 Å, and 3.03 Å, respectively. One carbon-hydrogen bond was identified with SER A:709 residues at a distance of 3.57 Å. Finally, two pi-alkyl interactions were identified with residues HIS A:759 and PHE A:1003 at distances of 4.61 Å and 4.67 Å, respectively (Figure **3**)

3.5.3. Docking with Tumor Necrosis Factor-alpha (TNF-α)

The molecular docking analysis of the active chemical constituents of Gt-BuOH, as identified by GC-MS, with the Tumor Necrosis Factor-alpha (TNF-α) protein revealed that Methyl butyrate acid interacts with the TNF-α protein, yielding a docking score of -3.2 kcal/mol. The interaction profile comprises two conventional hydrogen bonds with the GLY A:24 and GLY A:25 residues at distances of 2.21 Å and 2.24 Å, respectively. One pi-alkyl bond with PHE A:144 at a distance of 4.98 Å (Figure **4**).

Regarding the molecular docking of oleic acid methyl ester with the TNF-α protein, the docking score was -3.7 kcal/mol. The interaction profile comprises one alkyl bond between LEU A:57 and a residue at a distance of 4.39 Å. Five pi-alkyl bonds with two residues of TYR A: 59, two residues of TYR A: 119, and one residue from TYR A: 151 at distances of 4.29 Å, 4.58 Å, 4.40 Å, 5.35 Å, and 5.49 Å, respectively (Figure **4**).

During molecular docking of propanoic acid anhydride to the TNF-α protein, the docking score was -3.1 kcal/mol. The interaction profile includes three conventional hydrogen bonds with LEU A:26, ASN A:547, and ILE A:547 at distances of 2.06 Å, 2.45 Å, and 2.04 Å, respectively (Figure **4**).

For comparison, a molecular docking study was conducted to assess the interaction between the TNF-α protein and curcumin, a natural inhibitor of TNF-α. [60]. This yielded a docking score of -6.7 kcal/mol. The interaction profile delineates one conventional hydrogen bond involving TYR A:151 at a distance of 1.74 Å. One pi- sigma bond was identified with TYR A:119 residues at a distance of 3.76 Å. Finally, two pi-pi-stacked interactions were identified with residues TYR A:59 and TYR A:119 at distances of 4.04 Å and

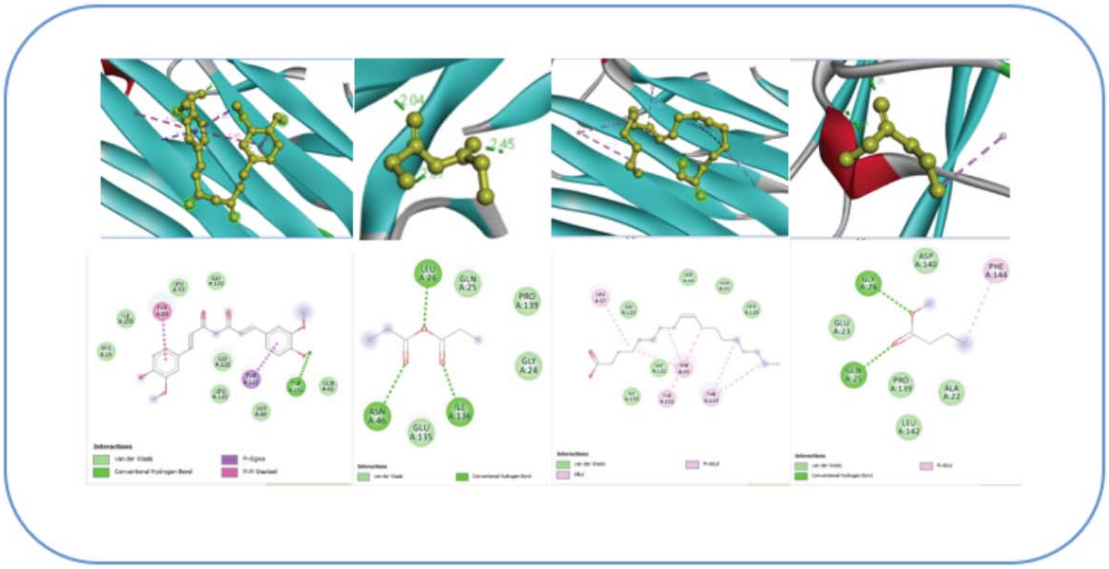


Figure 4: The structural configurations of the TNF-α binding sites are shown in both two-dimensional (upper image) and three-dimensional (lower image) views, illustrating the binding interactions with the following molecules from right to left (Methyl butyrate acid, oleic acid methyl ester, propanoic acid anhydride, and curcumin) with the TNF-α subunit.

5.03 Å, respectively (Figure **4**).

3.5.4. Comparative Analysis of Molecular Docking with Reference Inhibitors

The three Gt-BuOH constituents exhibited differential predicted binding affinities across the three targets. Methyl oleate consistently showed the highest predicted affinity among the three constituents for all targets (−5.7 to −3.7 kcal/mol), followed by propanoic anhydride (−5.5 to −3.1 kcal/mol) and methyl butyrate (−5.2 to −3.2 kcal/mol). However, all three constituents exhibited weaker predicted binding than the reference inhibitors: erlotinib (−7.1 kcal/mol for EGFR), etoposide (−8.1 kcal/mol for TOP2A), and curcumin (−6.7 kcal/mol for TNF-α) (Table **8**). The predicted affinities for the cancer-associated targets (EGFR and TOP2A; mean −5.40 to −5.67 kcal/mol) were higher than for TNF-α (mean −3.33 kcal/mol), but this differential binding pattern is hypothesis-generating only and does not constitute evidence of selective targeting or therapeutic advantage. No synergy or multi-target advantage is claimed.

3.7. Morphological Evaluation of Cytotoxicity

To validate the quantitative cytotoxicity data, morphology of both MCF-7 breast adenocarcinoma cells and normal HFF fibroblasts was evaluated using inverted phase-contrast microscopy after treatment. Fig. 5 (Panel A) shows that untreated control MCF-7 cells retained their typical epithelial-like morphology by assembling into cohesive, adhesive monolayers of polygonal, well-spread cells with distinct intercellular contacts—all hallmarks of active proliferation. In contrast, 1000 µg/mL Gt-BuOH exposure for 72 hours (Panel B) produced dramatic cytomorphological changes consistent with cell death. These features are characterized by prominent cell shrinkage, loss of the normal polygonal structure, blebbing of the plasma membrane, detachment from culture substrate and the appearance of round, non adherent rounding up and compacted cells which included all classical markers for apoptosis. Remarkably, the extent of morphological disturbance was similar to that evoked by the reference chemotherapeutic agent cisplatin (Panel C), which also induced massive cell rounding, substrate dissociation, and impaired monolayer integrity, thereby validating its established cytotoxic effect.

Simultaneously, morphological assessment of normal HFF cells (Figure **6**) revealed a distinctly different response. Untreated HFF cells (Panel A) displayed typical fibroblast morphology with spindle-shaped cells, extensive cytoplasmic extensions, and a confluent adherent monolayer. After 72-h treatment with 1000 µ g/mL Gt-BuOH (Panel B), HFF cells retained their characteristic shape and adherence, with no signs of shrinkage, rounding, or detachment. This structural preservation demonstrates the low cytotoxicity of Gt-BuOH toward normal fibroblasts, supporting the selective antiproliferative activity observed in the MTT assay and the favorable SI value. These visual observations suggest that Gt-BuOH preferentially affects cancer cells while sparing normal HFF cells under the conditions tested.

Table 8: Comparative Docking Scores (kcal/mol) of Gt-BuOH Phytoconstituents and Reference Inhibitors

Compound	EGFR (PDB: 1M17)	TOP2A (PDB: 5GWK)	TNF-α (PDB: 2AZ5)
Gt-BuOH Phytoconstituents			
Oleic acid methyl ester	-5.7	-6.3	-3.7
Propanoic acid anhydride	-5.4	-5.5	-3.1
Methyl butyrate acid	-5.1	-5.2	-3.2
Mean ± SD	-5.40 ± 0.30	-5.67 ± 0.58	-3.33 ± 0.32
Reference Inhibitors	Erlotinib: -7.1	Etoposide: -8.1	Curcumin: -6.7

Results are shown as binding affinity values (kcal/mol) calculated using AutoDock Vina, with lower values signifying stronger binding. Reference controls were composed of positive control ligands. Values are the lowest energy pose of all nine docking poses for the ligand-target pair. Values are mean ± SD for the three Gt-BuOH compounds. All three Gt-BuOH constituents exhibited weaker predicted binding affinities than the reference inhibitors. These docking scores are hypothesis-generating only and do not constitute evidence of functional inhibition or pharmacological synergy.

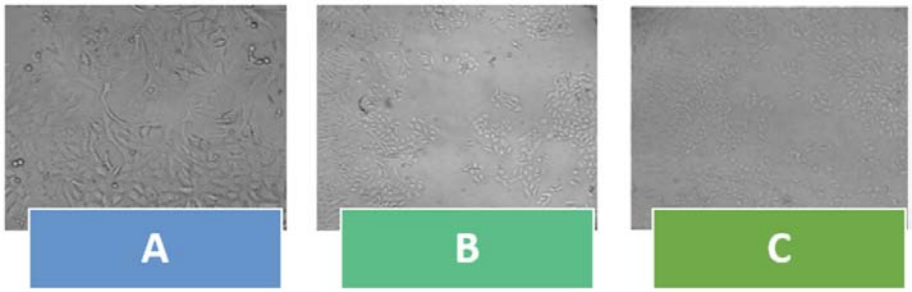


Figure 5: Morphological Features of MCF-7 Cells. The morphological features of MCF7 cells were examined utilizing an inverted microscope. The experimental groups consisted of: (**A**) untreated MCF7 cells used as controls; (**B**) MCF7 cells treated with 1000 µg/mL of Gt-BuOH for 72 hours; (**C**) MCF7 cells treated with 1000 µg/mL of cisplatin for 72 hours.

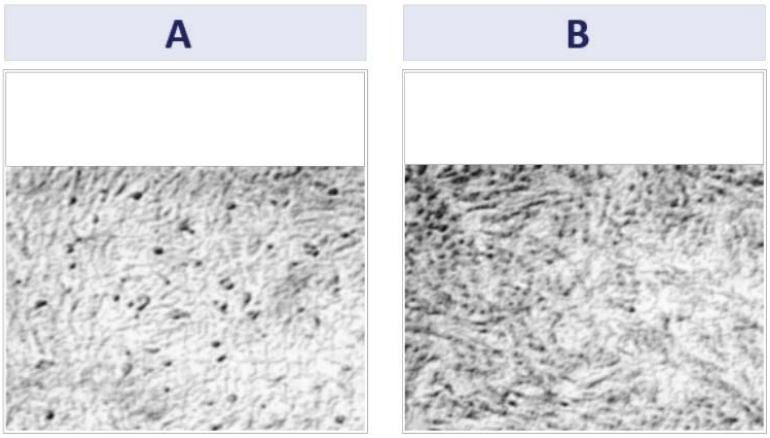


Figure 6: Morphological Features of HFF Cells. The morphological features of human foreskin fibroblast (HFF) cells were observed using inverted microscopy. Panel **A** depicts the untreated HFF cell line, whereas Panel **B** illustrates the cells after 72 hours of exposure to Gt-BuOH at 1000 µg/ml.

DISCUSSION

Breast cancer is still a leading cause of cancer death among women around the world, and other hormone-dependent subtypes, including MCF-7, are difficult to treat due to acquired drug resistance and off-target toxicity from standard chemotherapeutics [61]. There is an urgent need for safer, more selective anticancer agents, and natural products have received considerable attention in this context because many plant species remain unexplored [62]. This study used a multidisciplinary strategy, including cytotoxicity screening, ELISA-based biomarker analysis, and in silico molecular docking, to explore the anticancer effects of Gelasia tomentosa (formerly Scorzonera tomentosa), a perennial herbaceous species in the Asteraceae family. This integrated approach not only quantified biological activity but also enabled hypotheses surrounding potential molecular mechanisms and ultimately offered a basis to evaluate

the therapeutic feasibility of this plant extract. However, the findings should be interpreted as preliminary given the limited scope of the study.

Due to the widespread traditional use of Scorzonera sensu lato in folk medicine as an anti-inflammatory and cicatrizing agent, this genus represents a very interesting target for research focused on anticancer properties; however, systematic phytochemical and pharmacological studies evaluating cytotoxic potential are surprisingly few [54]. To our knowledge, this is the first study to examine the anticancer activity of G. tomentosa against breast cancer cell lines, contributing to the phytopharmacological characterization of this species. The choice of this plant was further justified by its extensive distribution in the Kurdistan region of Iraq and its ethnopharmacological relevance, providing a solid basis for analyzing its bioactive compounds.

The butanolic extract (Gt-BuOH) was chemically characterized by GC-MS, revealing a chemical profile mainly of long-chain unsaturated fatty acid methyl esters, such as methyl oleate (9-octadecenoic acid methyl ester), which accounted for 71.62% of the area of the total ion chromatogram area. This result agrees with the observed chemotaxonomic properties of members of Asteraceae, which habitually concentrate lipid-soluble compounds in their aerial organs [63]. Methyl oleate is particularly notable because it has demonstrated anticancer activity through various mechanisms, including induction of apoptosis, inhibition of cell proliferation, and regulation of lipid metabolism in cancer cells [64]. The identification of trace levels of propanoic anhydride, methyl butyrate, and butanoic acid methyl ester contributes to the extract's chemical complexity of this extract and may result in additive interactions that increase total biological activity [65]. The discovery of these short-chain fatty acid derivatives aligns with the species' metabolic flexibility and may be representative of adaptations to its extreme high-alpine habitat that would favour producing volatile, defensive metabolites. Importantly, the GC-MS profile does not support a phenolic-enriched composition; the bioactive constituents appear to be fatty-acid derivatives rather than phenolics. GC-MS without derivatization is poorly suited for detecting polar phenolics, and future UPLC-MS/MS analysis would be required to definitively assess phenolic content.

Cytotoxicity assessment showed that Gt-BuOH attenuated the growth of MCF-7 breast cancer cells in a dose- and time-dependent manner with an IC_{50} value of 431.8 µg/mL at 72 h but had minimal toxicity on normal HFF fibroblasts (IC_{50} > 1000 µg/mL). This differential cytotoxicity is therapeutically valuable, as it suggests preferential targeting of malignant cells over their non-malignant counterparts [66]. The potency enhancement over time, as indicated by a decrease in IC_{50} from 24 h to 72 h of treatment by 45%, suggests that the bioactive constituents may need time for their maximum cytotoxic effect to appear and may act through cumulative intracellular damage, or perhaps active induction of delayed apoptotic pathways [67]. These parallel data for an unmatched in vitro therapeutic index—the selective toxicity index (SI) (calculated using 72-h IC_{50} values)—provide additional evidence of Gt-BuOH safety within this model system compared to cisplatin with <0.11 SI, due to excessive normal HFF cell toxicity with the dose of cisplatin tested (IC_{50} = 112 µg/mL). However, the SI of >2.32 is modest, and the moderate IC_{50} of 431.8 µg/mL for a crude extract indicates that purification and identification of active principles would be required to achieve more significant therapeutic effects. Nevertheless, cisplatin showed unexpected potency against MCF-7 cells, and it was highly toxic to HFF cells, which may be explained by the experimental conditions: parenteral aqueous solutions of cisplatin are reported to be unstable, which may explain the results [68]. Moreover, the ineffectiveness of cisplatin towards MCF-7 cells contradicts the literature and indicates that this cell line may exhibit passage-specific or perhaps methodological resistance. This sharp contrast in selectivity highlights the possibility of plant-derived extracts being able to deliver therapeutic advantages in comparison with many conventional synthetic chemotherapeutics, which often possess a narrow therapeutic range and cytotoxicity limiting the maximum tolerated dose. Morphological analyses supported these quantitative observations: MCF-7 cells treated with Gt-BuOH exhibited classical apoptotic features such as cellular shrinkage and membrane blebbing followed by detachment, while HFF cells maintained their typical spindle-shaped morphology and a coherent monolayer in culture, confirming the selective nature of this extract's cytotoxic activity under the conditions tested.

Mechanistic information as to why Gt-BuOH has different effects on cancer compared to normal cells was also provided by the ELISA analysis. MCF-7 cells treated for 72 h with Gt-BuOH at its IC_{50} concentration (431.8 µg/mL) showed a 59.9% reduction in phosphorylated EGFR levels, suggesting attenuation of this key pro-survival pathway that is often

hyperactivated in many breast cancers [19]. However, cisplatin was tested at 112 µg/mL (its IC_{50} against HFF cells) rather than at an equi-effective concentration against MCF-7 cells, so direct comparison of biomarker modulation between Gt-BuOH and cisplatin is not valid. Cisplatin treatment was associated with a 22.9% reduction in p-EGFR levels in MCF-7 cells, but this difference may reflect the different concentrations used rather than superior activity of Gt-BuOH. Similarly, Gt-BuOH treatment was associated with a 66.3% reduction in TOP2A levels in MCF-7 cells, compared with a 33.7% reduction with cisplatin (112 µg/mL); again, the concentration difference limits direct comparison. TOP2A is an important enzyme for DNA replication and a recognized therapeutic target, and the reduction in TOP2A protein levels associated with Gt-BuOH treatment is consistent with the observed inhibition of proliferation and apoptotic morphology. However, ELISA measures total protein levels, not enzymatic activity; functional assays (e.g., DNA relaxation or decatenation assays) would be required to confirm inhibition of TOP2A catalytic function [24]. Notably, Gt-BuOH did not significantly alter p-EGFR or TOP2A levels in normal HFF cells, whereas cisplatin treatment increased expression of both proteins in normal fibroblasts, consistent with a stress-induced adaptive response to DNA damage that could contribute to this drug's off-target toxicity [55]. Moreover, MCF-7 cells treated with Gt-BuOH exhibited a decrease in TNF-α levels by 53.9% in cell lysates compared to untreated counterparts, which may be favorable if this translates into decreased inflammatory signaling (inflammatory signaling due to TNF-α has been shown to promote tumor progression), while similarly having no significant effect on TNF-α levels in normal cells [34], potentially preserving physiological cellular immune homeostasis. However, intracellular TNF-α levels represent the stored protein pool rather than secreted cytokine, and measurement of secreted TNF-α in culture supernatants would provide complementary information on functional cytokine release.

The molecular docking studies generated structural hypotheses regarding the biological activities observed in vitro by predicting how the three dominant Gt-BuOH phytoconstituents (i.e., methyl oleate, methyl butyrate, and propanoic anhydride) interact with putative target proteins. Methyl oleate exhibited the highest predicted binding affinity among the three constituents for EGFR (−5.7 kcal/mol) and TOP2A (−6.3 kcal/mol), with hydrophobic interactions involving VAL A:702, LEU A:820, and LEU A:694 in EGFR, and conventional hydrogen bonds with SER A:717 and ARG A:727 in TOP2A [61]. However, all three constituents exhibited weaker predicted binding affinities than the reference inhibitors (erlotinib, etoposide, and curcumin), and the docking scores are hypothesis-generating only. The predicted affinities for the cancer-associated targets (EGFR and TOP2A; mean −5.40 to −5.67 kcal/mol) were higher than for TNF-α (mean −3.33 kcal/mol), but this differential pattern does not constitute evidence of selective targeting or therapeutic advantage. No synergy or multi-target advantage is claimed. The previously presented combined binding ratio analysis has been removed because summing absolute docking scores is not a valid method for assessing synergy or multi-target advantage. The Chou-Talalay Combination Index method is not applicable to computational docking scores. If experimentally verified, polypharmacological action may offer advantages over single-agent therapies by limiting the probability of resistance development and allowing lower doses with better safety profiles [66]; however, this remains a hypothesis. This congruence of in silico and wet-lab experiments supports the computational approach while also suggesting prospective mechanistic insights into Gt-BuOH's anticancer activity [52]. Nonetheless, computational predictions such as these should be followed up experimentally via surface plasmon resonance (SPR), isothermal titration calorimetry (ITC), or enzymatic activity assays to assess actual binding and biological relevance.

The notable polypharmacology of the identified phytoconstituents suggests the possibility that the crude extract may be therapeutically more beneficial than its individual components—a phenomenon widely reported in herbal preparations [67]. Nonetheless, this must be experimentally confirmed to move beyond hypothesis. The ability of methyl oleate to engage primarily hydrophobic binding pockets in concert with the smaller organic acids that can form hydrogen bonds with catalytic residues may provide a means by which to obtain overall target engagement via complementary modes of interaction [52]. This multi-targeting mechanism of action, which may be additive or synergistic, is consistent with growing recognition that complex mixtures of natural products can achieve improved therapeutic results through network pharmacology [64]. Based on its favorable selective toxicity profile and predicted polypharmacological potential against cancer-specific proteins, G. tomentosa is a promising source of lead compounds for further development [50].

Several limitations should be considered when interpreting the results of this investigation. The *in vitro* nature of all assays makes it difficult to extrapolate these results directly to a physiological context because factors such as immune cell infiltration and stromal interactions cannot be faithfully modeled in monolayer cultures. The moderate IC_{50} values seen for Gt-BuOH indicate that bioactive constituents are present in the extract; to attain more significant therapeutic effects, purification and identification of specific active principles would require bioassay-guided fractionation. Furthermore, the study did not examine Gt-BuOH's effects on normal breast epithelial cells to assess more directly the extract's specificity for malignant over non-malignant mammary tissue. Only one cancer cell line (MCF-7) and one non-breast normal cell line (HFF) were used; future studies should include additional breast cancer subtypes (e.g., MDA-MB-231, SK-BR-3, T-47D) and normal breast epithelial cells (e.g., MCF-10A). The SI of >2.32 is encouraging but modest, and the IC_{50} of 431.8 µg/mL for a crude extract is moderate. The use of etoposide as a TOP2A docking reference has mechanistic limitations because etoposide interacts with DNA rather than binding directly to the TOP2A ATPase domain; future studies should use catalytic TOP2A inhibitors (e.g., ICRF-193, merbarone) or experimentally validate binding via SPR/ITC. Cisplatin was tested at a non-equi-effective concentration relative to the extract, limiting direct comparison of biomarker modulation.

Further studies involving *in vivo* models, pharmacokinetic profiling, verification of docking predictions (e.g., SPR, ITC), bioassay-guided fractionation to isolate active principles, and targeted mechanistic investigations (including functional assays on TOP2A activity as well as apoptosis confirmation) are needed to facilitate the clinical potential of G. tomentosa-derived anticancer compounds.

CONCLUSION

This study provides preliminary evidence that the n-butanol fraction from Gelasia tomentosa (Gt-BuOH) displays selective *in vitro* antiproliferative activity against MCF-7 breast adenocarcinoma cells with minimal cytotoxicity to normal HFF fibroblasts under the experimental conditions used. GC-MS profiling revealed that methyl oleate was the most abundant component identified in the extract, followed by propanoic anhydride, methyl butyrate, and butanoic acid methyl ester, thereby elucidating the phytochemical basis for action. The GC-MS data indicate a fatty-acid-derivative-rich extract and are not consistent with a phenolic-enriched profile; this should be considered when interpreting the extract's chemical character. The butanolic extract acted in a duration-dependent manner, as demonstrated by the IC_{50} = 431.8 µg/mL against MCF-7 cells after 72 h of exposure, and exerted a selectivity index of >2.32. Conversely, the unexpectedly low potency of cisplatin in MCF-7 cells and its high toxicological effect in HFF cells suggest that the experimental conditions must be explored more thoroughly.

Mechanistically, ELISA analyses indicated associations between Gt-BuOH treatment and reduced p-EGFR and TOP2A protein levels in cancer cells but not normal cells, while computer-assisted molecular docking predicted individual binding affinities that were weaker than those of reference inhibitors. The previously presented combined binding ratio analysis has been removed because summing absolute docking scores is not a valid method for assessing synergy or multi-target advantage; the Chou-Talalay Combination Index method is not applicable to docking scores. No synergy or multi-target advantage is claimed. The preferential in silico binding of cancer proteins over TNF-α is hypothesis-generating only. The use of etoposide as a TOP2A docking reference has mechanistic limitations because etoposide interacts with DNA rather than binding directly to the TOP2A ATPase domain; direct TOP2A binders should be validated experimentally using SPR, ITC, or enzymatic assays in future studies.

The identification of G. tomentosa as lead material for potential multi-target anticancer compounds requires further studies including bioassay-guided fractionation, experimental verification of docking predictions (e.g., SPR, ITC, enzymatic assays), functional assays verifying TOP2A activity, and apoptosis confirmation (e.g., annexin V/PI staining, caspase activity), as well as *in vivo* efficacy testing and pharmacokinetic profiling, before any clinical development for adjunctive or alternative therapy against breast cancer can be considered.

AUTHOR CONTRIBUTIONS

Design and development: Amjed Abbawe Salih, Youssef Shakuri Yasin, Azal Hamoody Jumaa

Gathering and organizing data: Youssef Shakuri Yasin, Ali Mala Khedir Galalaey, Shatha H. Shaker

Data analysis/interpretation: Ahmed Mohsin Abdulkhadim, Amenh Mohammed Abdulrahman.

Article composition: Waleed Khalid Ahmed, Youssef Shakuri Yasin, Azal Hamoody Jumaa

Critique the essay for significant ideas: Amjed Abbawe Salih, Ahmed Mohsin Abdulkhadim

Statistical analysis expertise: Youssef Shakuri Yasin, Azal Hamoody Jumaa

Ultimate article endorsement and guarantee:. Ali Mala Khedir Galalaey, Youssef Shakuri Yasin

ACKNOWLEDGEMENTS

The research team sincerely thanks the researchers and instructional staff at ICMGR/Al-Mustansiriyah University and the Iraqi National Cancer Research Centre/University of Baghdad for their invaluable support throughout this study. We also deeply appreciate the dedicated quality control team at Samarra Pharmaceutical Factory for kindly providing the essential drugs used in our research.

FINANCIAL SUPPORT AND SPONSORSHIP

Self-funded

CONFLICTS OF INTEREST

The authors declare no conflicts of interest.

DECLARATION OF GENERATIVE AI AND AI-ASSISTED TECHNOLOGIES IN THE WRITING PROCESS

The authors confirm they did not utilize any AI-generated or AI-assisted tools in their research.

ABBREVIATIONS

AUC = Area Under the Curve

BMI = Body Mass Index

CI = Confidence Interval

CRP = C-Reactive Protein

CT = Computed Tomography

GCP = Good Clinical Practice

HDL = High-Density Lipoprotein

HR = Hazard Ratio

ICU = Intensive Care Unit

IQR = Interquartile Range

ITT = Intention-to-Treat

LDL = Low-Density Lipoprotein

MRI = Magnetic Resonance Imaging

mRNA = Messenger Ribonucleic Acid

NIH = National Institutes of Health

OR = Odds Ratio

PCR = Polymerase Chain Reaction

RCT = Randomized Controlled Trial

RNA = Ribonucleic Acid

SD = Standard Deviation

SEM = Standard Error of the Mean

REFERENCES

[1] Abdelgalil AA, Al-Kahtani HM, Al-Jenoobi FI. Erlotinib. Profiles of Drug Substances, Excipients and Related Methodology. Elsevier 2020.

[2] Abdulla KN, Khudhur RK, Said AM, Jumaa AH, Yasin YS. Laetrile and methotrexate: A dual-drug approach to inhibiting cervical cancer cell proliferation. J Cancer Res Updates 2025; 14: 52-62. https://doi.org/10.30683/1929-2279.2025.14.06

[3] Abu-Bader SH. Using statistical methods in social science research: With a complete SPSS guide. Oxford University Press 2021. Print ISBN: 9780197522431.

[4] Akitsu T, Tsvetkova D, Yamamoto Y, Nakane D, Kostova I. From basics of coordination chemistry to understanding cisplatin-analogue Pt drugs. Curr Pharm Des 2023; 29: 1747-1774. https://doi.org/10.2174/1381612829666230809094251

[5] Aksu M. Colorimetric Cytotoxicity Assays. IntechOpen eBooks 2022.

[6] Al-Mahdwi TT, Said AM, Hade IM, Yasin YS, Jumaa AH. Synergistic cytotoxic impact of linagliptin-ciprofloxacin combination on cervical cancer cell line: insights into targeting heat shock protein 60. Asian Pac J Cancer Prev 2025; 26: 2117. https://doi.org/10.31557/APJCP.2025.26.6.2117

[7] Alassadi S, Pisani MJ, Wheate NJ. A chemical perspective on the clinical use of platinum-based anticancer drugs. Dalton Trans 2022; 51: 10835-10846. https://doi.org/10.1039/D2DT01875F

[8] Ali ML, Roky AH, Azad SAK, Shaikat AH, Meem JN, Hoque E, Ahasan AMF, Islam MM, Arif MSR, Mostaq MS. Autophagy as a targeted therapeutic approach for skin cancer: evaluating natural and synthetic molecular interventions. Cancer Pathog Ther 2024; 2: 231-245. https://doi.org/10.1016/j.cpt.2024.01.002

[9] Atanasov AG, Zotchev SB, Dirsch VM, Supuran CT. Natural products in drug discovery: advances and opportunities. Nat Rev Drug Discov 2021; 20: 200-216. https://doi.org/10.1038/s41573-020-00114-z

[10] Balasco N, Esposito L, Vitagliano L. Structural Biology in the AlphaFold Era: How Far Is Artificial Intelligence from Deciphering the Protein Folding Code. Biomolecules 2025; 15: 674. https://doi.org/10.3390/biom15050674

[11] Banerjee V, Sharda N, Huse J, Singh D, Sokolov D, Czinn SJ, Blanchard TG, Banerjee A. Synergistic potential of dual andrographolide and melatonin targeting of metastatic colon cancer cells: Using the Chou-Talalay combination index method. Eur J Pharmacol 2021; 897: 173919. https://doi.org/10.1016/j.ejphar.2021.173919

[12] Berman HM, Burley SK. Protein Data Bank (PDB): Fifty-three years young and having a transformative impact on science and society. Q Rev Biophys 2025; 58: e9. https://doi.org/10.1017/S0033583525000034

[13] Bianco G, Holcomb M, Santos-Martins D, Tillack A, Hansel-Harris A, Forli S. Reactive docking: A computational method for high-throughput virtual screenings of reactive species. J Chem Inf Model 2023; 63: 5631-5640. https://doi.org/10.1021/acs.jcim.3c00832

[14] Bray F, Laversanne M, Sung H, Ferlay J, Siegel RL, Soerjomataram I, Jemal A. Global cancer statistics 2022: GLOBOCAN estimates of incidence and mortality worldwide for 36 cancers in 185 countries. CA Cancer J Clin 2024; 74: 229-263. https://doi.org/10.3322/caac.21834

[15] Buranaamnuay K. The MTT assay application to measure the viability of spermatozoa: A variety of the assay protocols. Open Vet J 2021; 11: 251-269. https://doi.org/10.5455/OVJ.2021.v11.i2.9

[16] Cattrini C, Capaia M, Boccardo F, Barboro P. Etoposide and topoisomerase II inhibition for aggressive prostate cancer: Data from a translational study. Cancer Treat Res Commun 2020; 25: 100221. https://doi.org/10.1016/j.ctarc.2020.100221

[17] Chaudhari R, Fong LW, Tan Z, Huang B, Zhang S. An up-to-date overview of computational polypharmacology in modern drug discovery. Expert Opin Drug Discov 2020; 15: 1025-1044. https://doi.org/10.1080/17460441.2020.1767063

[18] Chaudhry G, Zeenia, Safdar N, Begum S, Akim A, Sung Y, Muhammad T. Cytotoxicity assays for cancer drug screening: methodological insights and considerations for reliable assessment in drug discovery. Braz J Biol 2024; 84: e284409. https://doi.org/10.1590/1519-6984.284409

[19] Chou T-C. Theoretical basis, experimental design, and computerized simulation of synergism and antagonism in drug combination studies. Pharmacol Rev 2006; 58: 621-681. https://doi.org/10.1124/pr.58.3.10

[20] Chou T-C. Mass-Action Law Dynamics Theory and Algorithm for Translational and Precision Medicine Informatics. Elsevier 2024.

[21] Darji P, Patel J, Patel B, Chudasama A, Joel P, Nalla S. Recent method to improve stability profile, pharmacokinetic and pharmacodynamic properties in anticancer drugs. World J Pharm Life Sci 2024; 10: 216-229.

[22] Dasari S, Njiki S, Mbemi A, Yedjou CG, Tchounwou PB. Pharmacological effects of cisplatin combination with natural products in cancer chemotherapy. Int J Mol Sci 2022; 23: 1532. https://doi.org/10.3390/ijms23031532

[23] Deng B, Kong W, Suo H, Shen X, Newton MA, Burkett WC, Zhao Z, John C, Sun W, Zhang X. Oleic acid exhibits anti-proliferative and anti-invasive activities via the PTEN/AKT/mTOR pathway in endometrial cancer. Cancers 2023; 15: 5407. https://doi.org/10.3390/cancers15225407

[24] Dzobo K. The role of natural products as sources of therapeutic agents for innovative drug discovery. Comprehensive Pharmacology 2022; 408. https://doi.org/10.1016/B978-0-12-820472-6.00041-4

[25] Eldereny MM, Elhawary EA, El-Gneady FF, Labib RM. A Comprehensive Review on Genus Asystasia: Folk Medicinal Uses, Phytoconstituents, and Pharmacological Activities. Chem Biodivers 2025; 22: e202403439. https://doi.org/10.1002/cbdv.202403439

[26] Ezghayer MA, Kadhim EJ. UPLC-ESI-MS/MS and Various Chromatographic Technique for Identification of Phytochemicals in Populus euphratica Oliv. Leaves Extract. Iraqi J Pharm Sci 2020; 29: 94-114. https://doi.org/10.31351/vol29iss1pp94-114

[27] Fatemi N, Karimpour M, Bahrami H, Zali MR, Chaleshi V, Riccio A, Nazemalhosseini-Mojarad E, Totonchi M. Current trends and future prospects of drug repositioning in gastrointestinal oncology. Front Pharmacol 2024; 14: 1329244. https://doi.org/10.3389/fphar.2023.1329244

[28] Freitas JA, Ccana-Ccapatinta GV, Da Costa F. LC-MS metabolic profiling comparison of domesticated crops and wild edible species from the family Asteraceae growing in a region of São Paulo state, Brazil. Phytochem Lett 2021; 42: 45-51. https://doi.org/10.1016/j.phytol.2021.02.004

[29] Ghasemi M, Liang S, Luu QM, Kempson I. The MTT assay: a method for error minimization and interpretation in measuring cytotoxicity and estimating cell viability. Cell Viability Assays: Methods and Protocols. Springer 2023. https://doi.org/10.1007/978-1-0716-3052-5_2

[30] Granda-Santos M, Reyna-Gonzales K, Torrejón-Valqui L, Valle-Epquín MG, Caetano AC, Díaz-Valderrama JR, Castro-Alayo EM, Cayo-Colca IS, Maicelo JL, Balcázar-Zumaeta CR. Characterization of Terpenoids in Aromatic Plants Using Raman Spectroscopy and Gas Chromatography–Mass Spectrometry (GC–MS). Int J Mol Sci 2025; 26: 11254. https://doi.org/10.3390/ijms262311254

[31] Guo L-Y, Xing X, Tong J-B, Li P, Ren L, An C-X. Qsar Aided Design of Potent Ret Inhibitors Using Molecular Docking, Molecular Dynamics Simulation and Binding Free Energy Calculation. Molecular Dynamics Simulation and Binding Free Energy Calculation 2024. https://doi.org/10.2139/ssrn.4886845

[32] Jang D-I, Lee A-H, Shin H-Y, Song H-R, Park J-H, Kang T-B, Lee S-R, Yang S-H. The role of tumor necrosis factor alpha (TNF-α) in autoimmune disease and current TNF-α inhibitors in therapeutics. Int J Mol Sci 2021; 22: 2719. https://doi.org/10.3390/ijms22052719

[33] Jilla T. The role of molecular docking in drug discovery: current approaches and innovations. Int J Zool Environ Life Sci 2025; 16-20. https://doi.org/10.70604/ijzels.v2i2.55

[34] Jiménez-González V, Benítez G, Pastor JE, López-Lázaro M, Calderón-Montaño JM. Evaluation of anticancer activity of 76 plant species collected in Andalusia (Spain) against lung cancer cells. Plants 2023; 12: 3275. https://doi.org/10.3390/plants12183275

[35] Khudhur RK, Yahiya YI, Majeed AH, Yasin YS, Jumaa AH. Scrutiny of the co-cytotoxic impact of metformin-omeprazole on the cervical cancer cell line and their aptitude to target heat shock 60. Asian Pac J Cancer Prev 2025; 26: 1353. https://doi.org/10.31557/APJCP.2025.26.4.1353

[36] Kopacz-Bednarska A, Król T. Cisplatin—Properties and clinical application. Oncol Clin Pract 2022; 18: 166-176. https://doi.org/10.5603/OCP.2022.0020

[37] Liechty C, Hu J, Zhang L, Liechty KW, Xu J. Role of microRNA-21 and its underlying mechanisms in inflammatory responses in diabetic wounds. Int J Mol Sci 2020; 21: 3328. https://doi.org/10.3390/ijms21093328

[38] Loibl S, Poortmans P, Morrow M, Denkert C, Curigliano G. Breast cancer. Lancet 2021; 397: 1750-1769. https://doi.org/10.1016/S0140-6736(20)32381-3

[39] Macari G, Toti D, Pasquadibisceglie A, Polticelli F. DockingApp RF: a state-of-the-art novel scoring function for molecular docking in a user-friendly interface to AutoDock Vina. Int J Mol Sci 2020; 21: 9548. https://doi.org/10.3390/ijms21249548

[40] Martinho N, Marques JM, Todoriko I, Prieto M, de Almeida RF, Silva LC. Effect of cisplatin and its cationic analogues in the phase behavior and permeability of model lipid bilayers. Mol Pharm 2023; 20: 918-928. https://doi.org/10.1021/acs.molpharmaceut.2c00321

[41] Matias Barrios VM. New catalytic topoisomerase II inhibitors discovered for anticancer therapeutics. University of British Columbia 2021. https://doi.org/10.3389/fonc.2020.633142

[42] Morais P, da Silva D. Mathematical Modeling for an MTT Assay in Fluorine-Containing Graphene Quantum Dots. Nanomaterials 2022; 12: 413. https://doi.org/10.3390/nano12030413

[43] Moreno Cardenas C, Grieco GMF, Zheleva-Dimitrova D, Appendino G, Zidorn C. Are Furanocoumarins Present in the

Cichorieae Tribe of Asteraceae A Comparative Study of Cicerbita alpina (Asteraceae) and Peucedanum ostruthium (Apiaceae). Plants 2025; 14: 2815. https://doi.org/10.3390/plants14182815

[44] Newman DJ, Cragg GM. Natural products as sources of new drugs over the nearly four decades from 01/1981 to 09/2019. J Nat Prod 2020; 83: 770-803. https://doi.org/10.1021/acs.jnatprod.9b01285

[45] Nilles J, Weiss J, Theile D. Crystal violet staining is a reliable alternative to bicinchoninic acid assay-based normalization. Biotechniques 2022; 73: 131-135. https://doi.org/10.2144/btn-2022-0064

[46] Nitiss JL, Kiianitsa K, Sun Y, Nitiss KC, Maizels N. Topoisomerase assays. Curr Protoc 2021; 1: e250. https://doi.org/10.1002/cpz1.250

[47] Nolan E, Lindeman GJ, Visvader JE. Deciphering breast cancer: from biology to the clinic. Cell 2023; 186: 1708-1728. https://doi.org/10.1016/j.cell.2023.01.040

[48] Özcan Aykutlu A, Makbul S, Coşkunçelebi K, Seyis F. Secondary volatile metabolite composition in Scorzonera pseudolanata Grossh. plant parts. Plants 2025; 14: 1624. https://doi.org/10.3390/plants14111624

[49] Özenver N, Efferth T. Integration of phytochemicals and phytotherapy into cancer precision medicine. Approaching Complex Diseases: Network-Based Pharmacology and Systems Approach in Bio-Medicine. Springer 2020. https://doi.org/10.1007/978-3-030-32857-3_16

[50] Peng Y, Ao M, Dong B, Jiang Y, Yu L, Chen Z, Hu C, Xu R. Anti-inflammatory effects of curcumin in the inflammatory diseases: status, limitations and countermeasures. Drug Des Devel Ther 2021; 4503-4525. https://doi.org/10.2147/DDDT.S327378

[51] Piepho HP. Letters in mean comparisons: What they do and don't mean. Agron J 2018; 110: 431-434. https://doi.org/10.2134/agronj2017.10.0580

[52] Pintor A, Queiroz L, Barcelos R, Primo L, Maia L, Alves G. MTT versus other cell viability assays to evaluate the biocompatibility of root canal filling materials: a systematic review. Int Endod J 2020; 53: 1348-1373. https://doi.org/10.1111/iej.13353

[53] Plant E. Bioprospecting Ethnomedicinal Plant Resources.

[54] Pommier Y, Nussenzweig A, Takeda S, Austin C. Human topoisomerases and their roles in genome stability and organization. Nat Rev Mol Cell Biol 2022; 23: 407-427. https://doi.org/10.1038/s41580-022-00452-3

[55] Pudziuvelyte L, Marksa M, Sosnowska K, Winnicka K, Morkuniene R, Bernatoniene J. Freeze-drying technique for microencapsulation of Elsholtzia ciliata ethanolic extract using different coating materials. Molecules 2020; 25: 2237. https://doi.org/10.3390/molecules25092237

[56] Saikia S, Puzari M, Chetia P. Molecular docking in drug designing and Metabolism. Industrial Microbiology and Biotechnology: Emerging Concepts in Microbial Technology. Springer 2023. https://doi.org/10.1007/978-981-99-2816-3_14

[57] Samolada S. 2.1 Chromatographic system instrumentation. Smartphones for Chemical Analysis: From Proof-of-concept to Analytical Applications 2023; 101: 279.

[58] Santa-María C, López-Enríquez S, Montserrat-de la Paz S, Geniz I, Reyes-Quiroz ME, Moreno M, Palomares F, Sobrino F, Alba G. Update on anti-inflammatory molecular mechanisms induced by oleic acid. Nutrients 2023; 15: 224. https://doi.org/10.3390/nu15010224

[59] Shetty SR, Yeeravalli R, Bera T, Das A. Recent advances on epidermal growth factor receptor as a molecular target for breast cancer therapeutics. Anticancer Agents Med Chem 2021; 21: 1783-1792. https://doi.org/10.2174/1871520621666201222143213

[60] Silvia N, Rao AS, Kranthi Y, Yohan G, Saketh D, Meghamala G, Kumar KP. Innovative Approaches for the Extraction, Purification, and Quantification of Polyphenols: A Comprehensive Review. Int J Pharm Investig 2025; 15. https://doi.org/10.5530/ijpi.20250192

[61] Tabatabaei MS, Ahmed M. Enzyme-linked immunosorbent assay (ELISA). Cancer Cell Biology: Methods and Protocols. Springer 2022. https://doi.org/10.1007/978-1-0716-2376-3_10

[62] Trovato E, Micalizzi G, Dugo P, Utczás M, Mondello L. Use of linear retention indices in GC-MS libraries for essential oil analysis. Handbook of Essential Oils. CRC Press 2020. https://doi.org/10.1201/9781351246460-8

[63] Valaperti A, Li Z, Vonow-Eisenring M, Probst-Müller E. Diagnostic methods for the measurement of human TNF-alpha in clinical laboratory. J Pharm Biomed Anal 2020; 179: 113010. https://doi.org/10.1016/j.jpba.2019.113010

[64] Vaou N, Stavropoulou E, Voidarou C, Tsakris Z, Rozos G, Tsigalou C, Bezirtzoglou E. Interactions between medical plant-derived bioactive compounds: Focus on antimicrobial combination effects. Antibiotics 2022; 11: 1014. https://doi.org/10.3390/antibiotics11081014

[65] Vohra P. Network Pharmacology: A Paradigm Shift in the Field of Drug Discovery and Screening. ARC AJPS 2022. https://www.ijaresm.com/network-pharmacology-a-paradigm-shift-in-the-field-of-drug-discovery

[66] Wink M. Current understanding of modes of action of multicomponent bioactive phytochemicals: potential for nutraceuticals and antimicrobials. Annu Rev Food Sci Technol 2022; 13: 337-359. https://doi.org/10.1146/annurev-food-052720-100326

[67] Zaika MA, Kilian N, Jones K, Krinitsina AA, Nilova MV, Speranskaya AS, Sukhorukov AP. Scorzonera sensu lato (Asteraceae, Cichorieae)–taxonomic reassessment in the light of new molecular phylogenetic and carpological analyses. PhytoKeys 2020; 137: 1. https://doi.org/10.3897/phytokeys.137.46544

[68] Zayed AOH. Optimizing protein-ligand Docking through machine learning: algorithm selection with AutoDock Vina. Discov Chem 2025; 2: 164. https://doi.org/10.3897/phytokeys.137.46544

Received on 21-09-2026 Accepted on 20-10-2026 Published on 14-11-2026

https://doi.org/10.30683/1929-2279.2026.15.35

© 2026 Salih *et al*.; Licensee Neoplasia Research.
This is an open-access article licensed under the terms of the Creative Commons Attribution License (http://creativecommons.org/licenses/by/4.0/), which permits unrestricted use, distribution, and reproduction in any medium, provided the work is properly cited.